PLOS COMPUTATIONAL BIOLOGY

RESEARCH ARTICLE

Integrated computational and *in vivo* models reveal Key Insights into macrophage behavior during bone healing

Etienne Baratchart[1‡], **Chen Hao Lo**[2,3‡], **Conor C. Lynch**[2‡*], **David Basanta**[1‡*]

1 Integrated Mathematical Oncology Department, SRB4, Moffitt Cancer Center and Research Institute, Tampa, Florida, United States of America, **2** Cancer Biology Ph.D. Program, Department of Cell Biology Microbiology and Molecular Biology, University of South Florida, Tampa, Florida, United States of America, **3** Tumor Biology Department, SRB3, Moffitt Cancer Center and Research Institute, Tampa, Florida, United States of America

‡ EB and CHL are co-first authors on this work. CCL and DB are co-senior authors on this work
* conor.lynch@moffitt.org (CL); david@cancerevo.org (DB)

Citation: Baratchart E, Lo CH, Lynch CC, Basanta D (2022) Integrated computational and *in vivo* models reveal Key Insights into macrophage behavior during bone healing. PLoS Comput Biol 18(5): e1009839. https://doi.org/10.1371/journal.pcbi.1009839

Editor: Dominik Wodarz, University of California Irvine, UNITED STATES

Received: November 19, 2020

Accepted: January 17, 2022

Published: May 13, 2022

Data Availability Statement: All relevant data are within the manuscript and its Supporting information files Data and code are available on the following repository: https://github.com/ebaratch/Code_Fit_Macrophages.git Data from in vivo bone injury experiment were derived from preprint manuscript available in the Cold Spring Harbor bioRxiv server, https://www.biorxiv.org/content/10.1101/2020.10.13.338335v1.abstract.

Funding: This work was supported by the National Institute of Health (https://www.nih.gov/) grants:

Abstract

Myeloid-derived monocyte and macrophages are key cells in the bone that contribute to remodeling and injury repair. However, their temporal polarization status and control of bone-resorbing osteoclasts and bone-forming osteoblasts responses is largely unknown. In this study, we focused on two aspects of monocyte/macrophage dynamics and polarization states over time: 1) the injury-triggered pro- and anti-inflammatory monocytes/macrophages temporal profiles, 2) the contributions of pro- versus anti-inflammatory monocytes/macrophages in coordinating healing response. Bone healing is a complex multicellular dynamic process. While traditional *in vitro* and *in vivo* experimentation may capture the behavior of select populations with high resolution, they cannot simultaneously track the behavior of multiple populations. To address this, we have used an integrated coupled ordinary differential equations (ODEs)-based framework describing multiple cellular species to *in vivo* bone injury data in order to identify and test various hypotheses regarding bone cell populations dynamics. Our approach allowed us to infer several biological insights including, but not limited to,: 1) anti-inflammatory macrophages are key for early osteoclast inhibition and pro-inflammatory macrophage suppression, 2) pro-inflammatory macrophages are involved in osteoclast bone resorptive activity, whereas osteoblasts promote osteoclast differentiation, 3) Pro-inflammatory monocytes/macrophages rise during two expansion waves, which can be explained by the anti-inflammatory macrophages-mediated inhibition phase between the two waves. In addition, we further tested the robustness of the mathematical model by comparing simulation results to an independent experimental dataset. Taken together, this novel comprehensive mathematical framework allowed us to identify biological mechanisms that best recapitulate bone injury data and that explain the coupled cellular population dynamics involved in the process. Furthermore, our hypothesis testing methodology could be used in other contexts to decipher mechanisms in complex multicellular processes.

U01CA202958 and U01CA244101 to DB and CL. The funders had no role in study design, data collection and analysis, decision to publish, or preparation of the manuscript.

Competing interests: The authors have declared that no competing interests exist.

Author summary

Myeloid-derived monocytes/macrophages are key cells for bone remodeling and injury repair. However, their temporal polarization status and control of bone-resorbing osteoclasts and bone-forming osteoblasts responses is largely unknown. In this study, we focused on two aspects of monocyte/macrophage population dynamics: 1) the injury-triggered pro- and anti-inflammatory monocytes/macrophages temporal profiles, 2) the contributions of pro- versus anti-inflammatory monocytes/macrophages in coordinating healing response. In order to test various hypotheses regarding bone cell populations dynamics, we have integrated a coupled ordinary differential equations-based framework describing multiple cellular species to *in vivo* bone injury data. Our approach allowed us to infer several biological insights including: 1) anti-inflammatory macrophages are key for early osteoclast inhibition and pro-inflammatory macrophage suppression, 2) pro-inflammatory macrophages are involved in osteoclast bone resorptive activity, whereas osteoblasts promote osteoclast differentiation, 3) Pro-inflammatory monocytes/macrophages rise during two expansion waves, which can be explained by the anti-inflammatory macrophages-mediated inhibition phase between the two waves. Taken together, this mathematical framework allowed us to identify biological mechanisms that recapitulate bone injury data and that explain the coupled cellular population dynamics involved in the process.

Introduction

The tightly-coupled relationship between bone-forming osteoblasts and bone-resorbing osteoclasts in bone remodeling and healing is well established [1]. Bone remodeling is initiated by osteoclastic turnover of aged and compromised bone tissue. Molecular cues derived from bone resorption subsequently drive mesenchymal precursor expansion and differentiation into osteoblasts for formation of new bone [1]. Bone healing on the other hand begins with osteoblastic bone callus deposition that is subsequently remodeled by osteoclasts [1]. Beyond this classic paradigm of the bone modeling unit (BMU), studies are increasingly identifying other cellular populations and factors that also contribute to the maintenance of bone. Macrophages of the myeloid lineage play critical roles in inflammation, wound healing and cancer progression [2]. Recent studies have also shed light on their contribution to bone biology. While osteoclasts have traditionally been known as the tissue resident macrophage of the bone, more recent studies identified a novel population of bone-resident macrophages, osteomacs, which facilitate osteoblast bone formation [3,4]. Additionally, in the context of bone healing, macrophages have been documented to rapidly infiltrate sites of bone injury to clear cellular debris in a process called efferocytosis and elicit subsequent inflammatory response and mineralized callus formation [1]. Monocytes and macrophages are major components of the bone immune infiltrate following injury [1,5–7]. Recent studies using genetic or pharmacological depletion of macrophages demonstrated significantly delayed time to bone repair [4,5,8–10]. The diversity of macrophage function owes to its versatility in polarizing and responding to environmental cues [1,6–8]. These critical functions ensure the right temporal sequence of events necessary for healthy and timely bone repair after injury. For instance, IL-4 and TNFα have been shown to promote different macrophage polarization states and impact bone healing [11–12]. As an example, acute pro-inflammatory factors such as TNFα can improve bone repair while prolonged administration has the opposite effect [11,12]. There are, however, a number of gaps in our understanding of monocyte and macrophage population and polarization behavior, including but not limited to: 1) the contributions of pro- versus

anti-inflammatory macrophages in coordinating bone injury response, 2) whether macrophages are directly involved in control of osteoclasts and osteoblasts populations and activities during bone injury, and 3) the main mechanisms that govern pro- and anti-inflammatory macrophages population dynamics.

While *in vitro* and *in vivo* experimentation techniques can capture the behavior of individual populations with high resolution, they do not allow for understanding the simultaneous interplay between multiple cell types whose numbers change over time. This obstacle can be overcome with the integration of experimental data to computational approaches in order to model the interactions occurring during bone injury repair. This type of approach has already been applied to other disease contexts like cancer [13–22]. Amongst the possible types of modeling approaches, agent-based models, such as discrete-continuum Hybrid Cellular Automata can examine mechanisms at the cellular scale leading to emergence of non-trivial macroscopic patterns [23]. One advantage of such an approach, is the possibility to inform the model with experimentally measured parameters. However, these parameters, such as macrophage polarization rate for example, can sometimes be exceptionally difficult to measure *in vivo* or *in vitro*. On the other hand, systems of Ordinary Differential Equations (ODEs) model individual populations over time under a well-mixed assumption and are often used to estimate *in vivo* parameters. While they do not describe cellular mechanisms as finely as agent-based models, their relative computational simplicity make them a convenient tool to identify key parameters through data fitting [24–26]. Multiple mathematical approaches have been used to study bone remodeling and repair [27–31]. The vast majority use systems of ODEs to model bone cell populations in homeostatic bone remodeling and bone disease such as osteoporosis and multiple myeloma [32–37]. Bone remodeling is a physiological program that is tightly regulated spatially and temporally. Other groups have considered the role of space in the process and represented cell population either as continuous spatial field, describing the dynamics by a set of partial differential equations (PDE) [38,39], or as individual agents by an agent-based model approach [22]. These models have largely focused on the interaction between bone-building osteoblasts and bone-resorbing osteoclasts, mostly ignoring the role of immune and inflammatory cells. Although these models have addressed biologically and clinically relevant questions, very few studies, one of which is from our group [40] have quantitatively compared predictions of bone injury dynamics to longitudinal biological data. Some studies have included the role of inflammatory cells like macrophages, but they remain theoretical and have not been experimentally validated [41,42]. The role of inflammation, and that of macrophages in particular, is recognized as being key for coordinating the bone injury response *in vivo* but, to date, how monocyte/macrophage populations coordinate it and interact directly with osteoblasts and osteoclasts (and vice versa) during bone remodeling has not been thoroughly examined [1,6]. Here we use experimental, in combination with published data, to integrate osteoblasts, osteoclasts, bone, naïve, pro- and anti-inflammatory monocytes and macrophages into a coupled ODE model of the bone ecosystem. This approach allowed for the interrogation of key hypotheses that explain the bone healing program, such as the polarization and clearance dynamics of monocytes/macrophages, interactions between anti-inflammatory macrophages and pro-inflammatory monocytes/macrophages, and how pro- and anti-inflammatory monocytes/macrophages modulate osteoclast and osteoblast behaviors. We posit this integrated approach can be used to uncover mechanisms driving bone injury repair dynamics and to identify key strategies aimed at shortening bone healing times.

Results

Quantitative data of cell populations during bone injury repair dynamics

During non-critical bone injury healing, the following sequence of steps occur: early inflammation and hematoma formation, direct intramembranous bone deposition into a mineralized callus by osteoblasts [43–45], and callus remodeling by osteoclasts [1,3,9,46]. Bone-forming osteoblasts and bone-resorbing osteoclasts are critical mediators of these steps, and their numbers shift accordingly during each phase of repair. In order to temporally quantitate bone cells during injury, we extracted multi-cellular longitudinal data from an experimental model of bone injury repair whereby non-critical epiphyseal fracture was generated in mice by direct intratibial injection [40,46–49] (Fig 1A). In the injured tibias of the mice, bone volume and cell populations numbers were quantified at baseline (day 0) and at day 1, 2, 3, 7 and 14 (n = 5/time point) following injury. High-resolution μCT analysis of the site of bone injury demonstrated changes in bone volume (BV/TV) subsequent to bone injury (Fig 1B). Bone volume remained diminished over a 48-hour period prior to a five-day long expansion, beyond

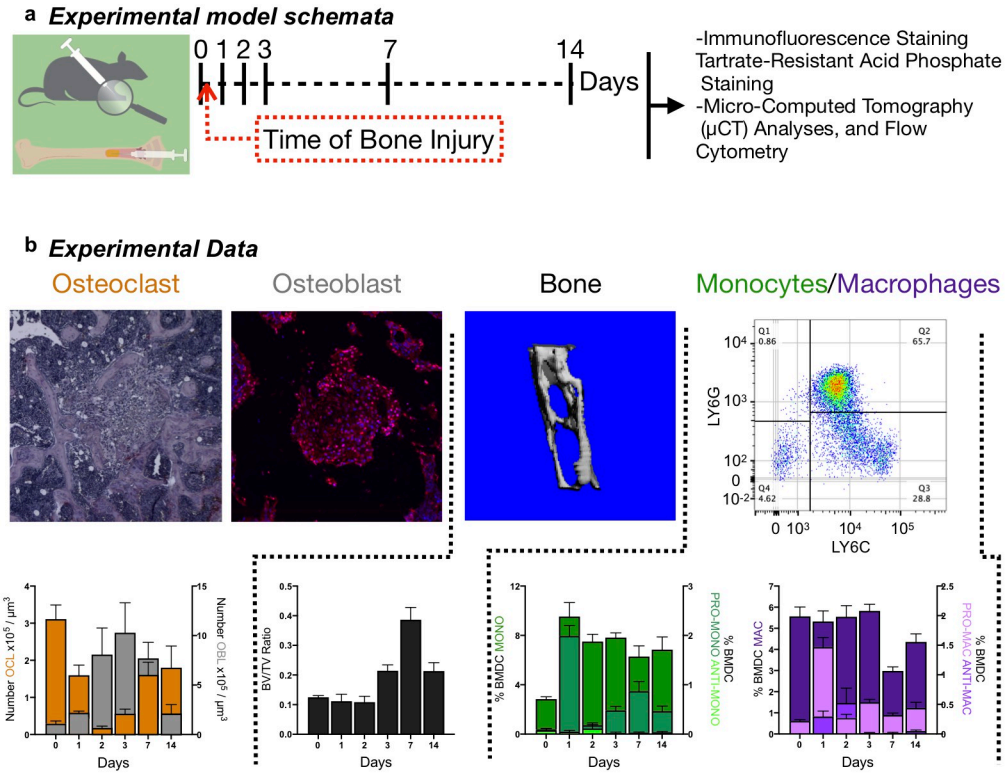

Fig 1. Experimental quantification of osteoblast, osteoclast, bone volume, and monocyte-macrophage over time during bone injury. a schematic summarizing the experimental system and the time course and different measurements performed. **b** from left to right: Decalcified bones were stained and quantified for OCL by tartrate-resistant acid phosphatase (TRAcP) staining (top left panel; red). Temporal quantification of OCL population was then assessed (bottom left panel); Decalcified bones were stained and quantified for OBL by RUNX2 immunofluorescence staining (second top panel; red). Temporal quantification of OBL population was then assessed (bottom left panel); micro-computed tomography revealed trabecular bone status. Representative images (third top panel) and corresponding quantitative analyses of bone volume on the top panel (BONE; BV/TV, second bottom panel). Flow cytometry was to gate and quantify monocytes-macrophages by the use of CD11b, Ly6C, Ly6G markers (Top right panel). Temporal quantification of naïve, pro-inflammatory and anti-inflammatory monocytes-macrophages populations was then assessed (bottom right panel).

https://doi.org/10.1371/journal.pcbi.1009839.g001

baseline levels. By day 14, the bone volume returned toward homeostasis. Consistent with other published observations, the overall bone volume dynamics were accompanied by corresponding sequential waves of osteoblast and osteoclast numbers [49–51] (Fig 1B). Interestingly, the overlaid data reveal alternating waves of osteoblasts and osteoclasts. In the same longitudinal study, the contralateral tibia from each mouse was additionally subject to flow cytometry to derive dynamics of total and polarized myeloid populations [2,4,5,7,52–105] (Fig 1B). The myeloid dataset shows that pro-inflammatory monocytes and macrophages spiked within the first 48 hours while anti-inflammatory macrophages were observed between 24 and 72 hours (Fig 1B). Importantly, a fainter but prolonged secondary wave of pro-inflammatory monocytes-macrophages was noted, an observation which is in line with past studies in other inflammatory contexts [51,106–108].

Mathematical modeling reveals key insights into myeloid behaviors during bone injury repair

In order to shed light on monocyte-macrophage dynamics, we interrogated hypotheses regarding population dynamics, differentiation, lifespan and plasticity. To this end we built a coupled ordinary differential equations-based framework describing seven cell populations as well as the bone volume temporal dynamics. The cell populations we considered in the model were bone-building osteoblasts, bone-resorbing osteoclasts, naïve monocytes, pro-inflammatory monocytes, naïve macrophages, pro and anti-inflammatory macrophages. To properly integrate cell population temporal data into this framework, we first curated common literature observations and hypotheses regarding osteoblasts, osteoclasts, monocyte and macrophage behavior during tissue injury healing (Table 1). In the model, the initial dynamics (osteoblast expansion, osteoclast decrease, macrophage polarization, monocyte infiltration) are triggered by injury factors [106]. We assume that the amount of factors released from an injury are proportional to the bone damage induced and are the primary driver of myeloid response. Myeloid cells are known to infiltrate the bone and polarize into pro-inflammatory status to clear cellular debris when exposed to injury-associated factors (Table 1) [1]. Therefore, an injury variable was included in the model that drives the initial pro-inflammatory response by monocytes/macrophages. In the model, this injury variable is being depleted by a decay rate term that is proportional to the number of pro-inflammatory cells (Equations on S1 and S3 Figs).

Table 1. Reference sources of predominant mechanisms. Established biological behaviors and functions of bone cell populations. Framework for a comprehensive and coupled 9-population ODE model is constructed based off of summarizing known published interactions between each population. Inclusion of select hypotheses for each ambiguous aspect of myeloid biology is based on the prevalence of their corresponding publications (at least seven supporting references for each).

Description	Fig 2 reference	PMID
Anti-inflammatory macrophages suppress osteoclast activity (Fig 2A1)	**a1**	[7,81,86,98,113,114,133,134]
Osteoclast and osteoblast activity are coupled (Fig 4A2 and 4A3)	**a2-3**	[4,49,112,114,134–145]
Anti-inflammatory macrophages induce osteoblast expansion	**b1**	[2–4,8–11,49,93,98,117,143,146]
Osteoblasts expand in response to bone injury and infection	**b2**	[3,4,8–11,49,93,112,114,117,142,143]
Bone injury induces inflammation and monocyte and macrophage polarization	**c1-3**	[4,7,11,69,94,111,140,141,143,147–150]
Anti-inflammatory cells suppress inflammation and pro-inflammatory cells	**c1-2**	[10,11,68,76,89,94,96,134,139,150,151]
Pro-inflammatory drive anti-inflammatory polarization of naïve myeloid cells	**c2**	[7,68,76,86,89,96,149]
Pro-inflammatory myeloid cells can repolarize to anti-inflammatory state	**c3**	[7,68,86,89,96,147,148]
Pro-inflammatory osteal macrophages induce inflammatory monocyte recruitment	**c3**	[4,8,11,73,76,84,89,94,95,139,142,143,147,152]
Polarized myeloid cells remove cellular debris, apoptotic cells and clear infection	-	[2,95,148,153,11,58,76,84,87,89,93,94,96,139,146,149,154]
Monocyte/macrophage are osteoclast precursors	-	[4,8,81,111,112,116,134,135,137–140,143,155,156]
Bone injury recruits inflammatory monocytes from circulation	-	[4,9–11,69,84,93,111,139,141,142,147,148,151,157]

https://doi.org/10.1371/journal.pcbi.1009839.t001

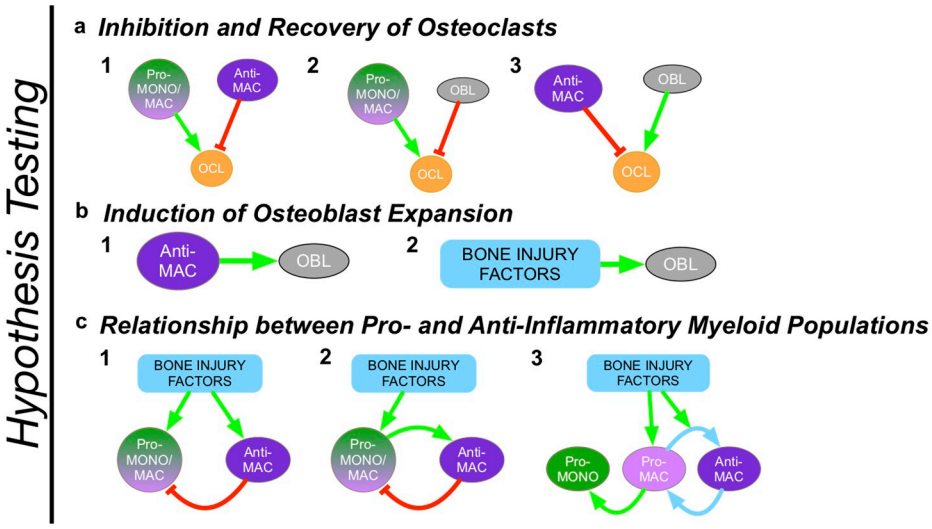

Fig 2. Comprehensive combinatorial modeling pipeline is built to identify relevant myeloid behaviors necessary to recapitulate *in vivo* bone injury repair data. Literature curation reveals sets of well-established competing biological mechanisms potentially governing modulation of osteoclast formation (**a**), regulation of osteoblast formation (**b**), and relationships between pro- and anti-inflammatory myeloid cells (**c**). Model adopts all combinations of hypotheses regarding these mechanisms to recapitulate *in vivo* data. Comparing model fits resulting from each hypothesis combination reveals best-fitting models.

https://doi.org/10.1371/journal.pcbi.1009839.g002

Browsing existing literature (Table 1), we identified various hypotheses regarding monocyte/macrophage control of osteoclast and osteoblast numbers, and the mechanistic relationship between pro- and anti-inflammatory myeloid cells (Fig 2 and Table 1). These hypotheses pertain to these three aspects of cell population dynamics:

1. Osteoclast dynamics
    a. Pro-inflammatory monocytes/macrophages stimulate osteoclast expansion; Anti-inflammatory monocytes/macrophages inhibit osteoclast formation and life span
    b. Pro-inflammatory monocytes/macrophages stimulate osteoclast expansion; Osteoblasts inhibit osteoclast formation and life span
    c. Osteoblasts stimulate osteoclast expansion; Anti-inflammatory macrophages inhibit osteoclast formation and life span
2. Osteoblast dynamics
    a. Anti-inflammatory factors stimulate osteoblast expansion
    b. Injury factors stimulate osteoblast expansion
3. Monocyte-Macrophage dynamics
    a. Injury factors drive both pro-inflammatory monocytes/macrophages and anti-inflammatory macrophages polarization; Anti-inflammatory macrophages suppress pro-inflammatory macrophages
    b. Injury factors drive pro-inflammatory monocytes/macrophages polarization; Pro-inflammatory monocytes/macrophages drive anti-inflammatory macrophages polarization; Anti-inflammatory macrophages suppress pro-inflammatory macrophages

c. Injury factors drive resident pro-inflammatory macrophages polarization; pro-inflammatory macrophages repolarize into anti-inflammatory macrophages when phagocytosing cellular debris; Anti-inflammatory macrophages naturally repolarize into pro-inflammatory macrophages in absence of stimulus (plasticity); Pro-inflammatory macrophages drive pro-inflammatory monocyte polarization.

Whereas evidence for all these mechanisms have been shown *in vitro* or *in vivo*, our goal here is to identify the ones that can recapitulate *in vivo* dynamics, in order to define main mechanisms that drive bone injury dynamics. We focus here on parsimonious hypothesis combinations, where for a given cell dynamics aspect (a, b or c), one mechanism only is considered, e.g c1 as opposed to c1&2.

We described the hypotheses using ordinary differential equations and integrated them into a mathematical model framework to assess the ability of each hypothesis combination to recapitulate the experimental data. This resulted in 18 ODE models, each describing a unique combination of hypotheses. In each permutation, we assessed how well the model fitted to the experimental data (Table 2). The models were ranked based on their goodness of fit, which was measured by the Akaike Information Criterion (AIC, Table 2), and number of residuals lower than 1 (Table 3). The fits to experimental data were obtained in two different ways, with the choice of two different functionals to minimize, J_2 and J_∞. Here we present the results obtained with J_∞ but the conclusions remained the same with J_2. Results indicate hypotheses combination *a3-b2-c2* (AIC of 39, Fig 3, equations presented in S1 Fig) shows the best fit to experimental data. The second, third and fourth best fits were obtained by *a3-b1-c2* (AIC of 42, S2 Fig), then a3-b1-c1 (AIC of 45, S4 Fig) and a3-b2-c1 (AIC of 46, S5 Fig). The AICs of

Table 2. Akaike information criterion (AIC) for comprehensive ODE of all 18 combinations of hypotheses. Akaike information criterion (AIC) for comprehensive ODE of all 18 combinations of hypotheses. Left columns denote the hypotheses from each of three mechanisms tested. The AIC scores resulting from J_2 and J_∞ minimization for each model are shown on the right and vary dramatically across models. Comparing AICs reveal one best combination (boxed in red) and the worst fitting model is highlighted in blue lines.

Mechanism Hypothesis			J_2	J_∞
a	***b***	***c***	**AIC Score**	**AIC Score**
1	*1*	*1*	79	73
1	*2*	*3*	77	68
1	*1*	*3*	78	67
1	*2*	*1*	79	73
1	*1*	*2*	89	70
1	*2*	*2*	115	65
2	*2*	*1*	81	76
2	*1*	*1*	103	79
2	*1*	*2*	78	69
2	*1*	*3*	78	66
2	*2*	*2*	88	78
2	*2*	*3*	128	113
3	*1*	*1*	58	45
3	*1*	*3*	76	56
3	*2*	*1*	57	46
3	*2*	*3*	86	59
3	*1*	*2*	51	42
3	***2***	***2***	**44**	**39**

https://doi.org/10.1371/journal.pcbi.1009839.t002

Table 3. Residuals lower than one for comprehensive ODE of all 18 combinations of hypotheses. Estimated parameters of the two best-fitting models. First column is the parameter notation used in the equations. Second column is the biological meaning of the parameter. Third and fourth columns are the parameter values for both models. Fifth column is the parameter unit. Sixth column is the reference used for retrieving parameter value, when it was possible/available. Parameters for which no reported estimation could be found were estimated by fitting on experimental data.

Mechanism Hypothesis			J_2	J_∞
a	***b***	***c***	**Residulas<1**	**Residulas<1**
1	*1*	*1*	18/40	14/40
1	*2*	*3*	16/40	12/40
1	*1*	*3*	20/40	15/40
1	*2*	*1*	15/40	14/40
1	*1*	*2*	12/40	14/40
1	*2*	*2*	9/40	13/40
2	*2*	*1*	18/40	11/40
2	*1*	*1*	15/40	12/40
2	*1*	*2*	18/40	17/40
2	*1*	*3*	20/40	15/40
2	*2*	*2*	16/40	15/40
2	*2*	*3*	8/40	8/40
3	*1*	*1*	16/40	13/40
3	*1*	*3*	13/40	14/40
3	*2*	*1*	17/40	14/40
3	*2*	*3*	16/40	19/40
3	*1*	*2*	21/40	15/40
3	***2***	***2***	**27/40**	**25/40**

https://doi.org/10.1371/journal.pcbi.1009839.t003

the remaining combinations were substantially lower (Table 2). Looking to another metric of goodness of fit, the number of residuals lower than 1, *a3-b2-c2* is clearly the best combination, with 25 residuals lower than one, and the rest of the models is far apart. With 15, 13 and 14 residuals lower than one, respectively, *a3-b1-c2*, a3-b1-c1 and a3-b2-c1 rank pretty low regarding to the residuals metric (Table 3). Interestingly, some hypothesis combinations do better than *a3-b1-c2*, a3-b2-c1 and a3-b1-c1 in term of number of residuals lower than 1, but worst in term of AIC. In conclusion, combination *a3-b2-c2* does substantially better than all other combinations for both goodness of fit criteria (and for both J_2 and J_∞ optimizations). Of note, the best-fitting hypothesis *a3-b2-c2* (Fig 3) assumes osteoblasts are the main osteoclastogenesis driver (Fig 2 Hypothesis *a3*), and that anti-inflammatory macrophages play an important role in suppressing osteoclasts and pro-inflammatory macrophages [91] (Fig 2 Hypothesis *c2*). It also suggests that initial osteoblast expansion is driven by factors associated with the onset of bone injury [106]. The coupled mathematical model also allows for the estimation of polarization rates over time for pro-and anti-inflammatory macrophages in these two scenarios (Table 4). By comparison, some hypotheses combinations such as *a2-b2-c3* yielded significantly poorer fits (AIC of 113 for *a2-b2-c3*, the worst fitting one, Table 2 and Fig 4, AIC of 79 for *a2-b1-c1*, the second worst fitting one, Table 2 and S6 Fig). This last result demonstrates that some cellular mechanisms and behaviors, though well-established in orthopedics (e.g. osteoclast stimulation by pro-inflammatory monocytes/macrophages; osteoclasts inhibition by osteoblasts through signals like OPG) are not able to recapitulate experimental observations in specific physiological contexts. Taken together, these results show, through our integrative hypothesis combination testing framework, the minimal set of cell-cell behaviors necessary to recapitulate bone injury temporal dynamics.

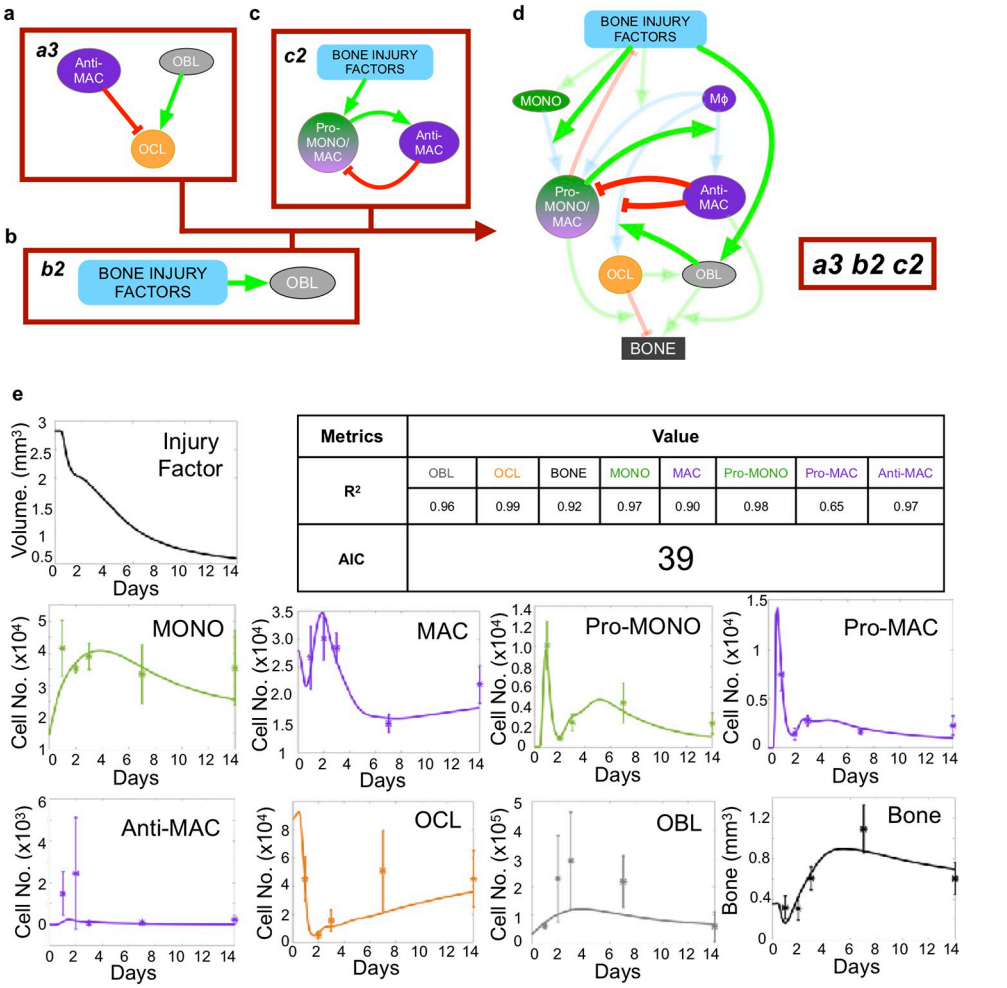

Fig 3. The best fitting hypothesis combination model integrates hypotheses *a3*, *b2* and *c2* (red boxes in **a**-**c**). **a** mechanism *a3* assumes that osteoblasts and anti-inflammatory macrophages promote and inhibit osteoclast formation, respectively. **b** mechanism *b2* assumes that injury factors promote osteoblast expansion. **c** mechanism *c2* assumes that injury factors promote pro-inflammatory monocytes/macrophages polarization. Pro-inflammatory monocytes/macrophages promote anti-inflammatory macrophages polarization, which in return drive depolarization of monocytes/macrophages back to the naive state. **d** schematic representation of the model using *a3-b2-c2* hypothesis combination. Arrows represent positive (green) or negative (red) types of cellular interactions. **e** Temporal plots and corresponding goodness of fit metrics (AIC and R2s) across all populations, obtained through J_{∞} minimization.

https://doi.org/10.1371/journal.pcbi.1009839.g003

Model simulations are consistent with independent published experimental data

Analysis of the literature reveals several factors that are important regulators of bone injury repair, such as tumor necrosis factor alpha (TNFα), interleukin-4 (IL-4), interferon-γ (IFNγ) and oncostatin M (OSM) [69,98,109–116]. For example, studies in mice genetically deficient for OSM exhibited reduced bone formation and osteoblasts numbers at the non-critical bone injury site [49,117]. OSM is produced by anti-inflammatory macrophages and promotes osteoblast expansion and activity [49,117–119]. To assess the robustness of our bone injury repair mathematical model we simulated the effect of OSM depletion on osteoblast number and determined if the model would recapitulate the qualitative temporal dynamics of osteoblast, osteoclast population and bone volume as shown in an independent experimental dataset [49].

Table 4. Parameter values of the best fitting model a3b2c2. Table showing biological description of each mathematical variable with data-derived initial conditions and units. First column is the variable notation used in the equations for each parameter. Second column is the biological meaning of the variable. Third column is the initial condition for each variable, typically an initial cell population level. Fourth column is the variable unit.

Parameter	Description	Value	Unit	Reference
		a3 b2 c2		
δ_{Mo}	Monocyte Lifespan	0,45	Day^{-1}	[158]
δ_{M}	Macrophage Lifespan	0,1	Day^{-1}	[159]
δ_{OB}	Bone-mediated Osteoblast lifespan	0,32	Day^{-1}	Estimated
δ_{OC}	Osteoclast lifespan	0,53	Day^{-1}	[160]
γ_{OB}	Macrophage-mediated Osteoblast Formation Rate	4.33×10^{4}	$Cell\ mm^{-3}\ Day^{-1}$	Estimated
δ_{B}	Per Bone Volume Unit Homeostatic Resorption Rate	5.99×10^{-7}	$Cell^{-1}\ Day^{-1}$	Estimated
Π_{B}	Homeostatic Bone Apposition Rate	6.018×10^{-7}	$mm^{3}\ Cell^{-1}\ Day^{-1}$	Determined from δ_B
α	Modulation of Resorption Rate by Pro-inflammatory Cell	0,0022	$Cell^{-1}$	Estimated
β	Modulation of Apposition Rate by Anti-inflammatory Cell	0,012	$Cell^{-1}$	Estimated
H_{Mo}	Homeostatic Monocyte Formation Rate	1.5×10^{4}	$Cell\ Day^{-1}$	Estimated
H_{M}	Homeostatic Macrophage Formation Rate	1.8×10^{4}	$Cell\ Day^{-1}$	Estimated
H_{OB}	Homeostatic Osteoblast Formation Rate	0,014	$Cell\ Cell^{-1}\ Day^{-1}$	Determined from δ_{OB}
d_{OC}	Osteoblast-mediated Osteoclast Formation Rate	5.35×10^{-5}	$Cell^{-1}\ Day^{-1}$	Determined from δ_{OC}
$Inhib_{OC}$	Macrophage-mediated Osteoclast inhibition	0,016	$Cell^{-1}$	Estimated
$Inhib_{OC2}$	Macrophage-mediated Osteoclast inhibition	0,052	$Cell^{-1}$	Estimated
δ_{D}	Macrophage/Monocyte-mediated debris clearance	1.71×10^{-5}	$Cell^{-1}\ Day^{-1}$	Estimated
I_1	Pro-Inflammatory cells-mediated monocyte recruitment	1.21×10^{-22}	$Cell\ Cell^{-1}\ Day^{-1}$	Estimated
I_2	Injury signals-mediated monocyte recruitment	6.15×10^{3}	$Cell\ mm^{-3}\ Day^{-1}$	Estimated
p_{31}	Injury Factors-mediated Pro-inflammatory Monocytes Polarization Rate	6.094×10^{-73}	$mm^{-3}\ Day^{-1}$	Estimated
p_{32}	Pro-inflammatory Cells-mediated Pro-inflammatory Monocytes Polarization Rate	3.42×10^{-5}	$mm^{-3}\ Cell^{-1}\ Day^{-1}$	Estimated
$depol_3$	Pro-inflammatory Monocytes depolarization Rate	0,029	$Cell^{-1}\ Day^{-1}$	Estimated
p_{11}	Injury Factors-mediated Pro-inflammatory M Polarization Rate	5.86×10^{-9}	$mm^{-3}\ Day^{-1}$	Estimated
p_{12}	Pro-inflammatory Cells-mediated Pro-inflammatory Macrophages Polarization Rate	4.69×10^{-4}	$mm^{-3}\ Cell^{-1}\ Day^{-1}$	Estimated
p_2	Anti-Inflammatory Macrophages Polarization Rate	2.34×10^{-6}	$Cell^{-1}\ Day^{-1}$	Estimated
$depol_1$	Pro-inflammatory Macrophages depolarization Rate	0,37	$Cell^{-1}\ Day^{-1}$	Estimated
$depol_2$	Anti-inflammatory Macrophages depolarization Rate	1.47×10^{-39}	Day^{-1}	Estimated

https://doi.org/10.1371/journal.pcbi.1009839.t004

We found that reducing the effect of anti-inflammatory macrophages on osteoblast expansion by 50%, mineralization activity by 50% and osteoclast inhibition by 80% yielded similar osteoblast, osteoclast and bone dynamics to those obtained from the OSM-deficient mice (Fig 5). Of note, osteoblast and bone levels are below baseline osteoclast number and remain largely unchanged between treatment and control in both the experimental data and model predictions. While not examined *in vivo* by the independent study, our mathematical model additionally generated corresponding predictions of the effect of OSM depletion on monocyte/macrophage dynamics (Fig 5). Interestingly, OSM depletion increased anti-inflammatory macrophage population and transiently decreased pro-inflammatory populations. Collectively, our model predictions are in qualitative accordance with this independent experimental dataset. This suggests that the model can be used for understanding the roles of myeloid cells in the bone ecosystem during bone injury healing and for developing therapies to accelerate and improve the process.

Discussion

Much remains to be discovered about how cells in the bone ecosystem collectively orchestrate the bone injury repair. Pharmacological and genetic experimental approaches can provide

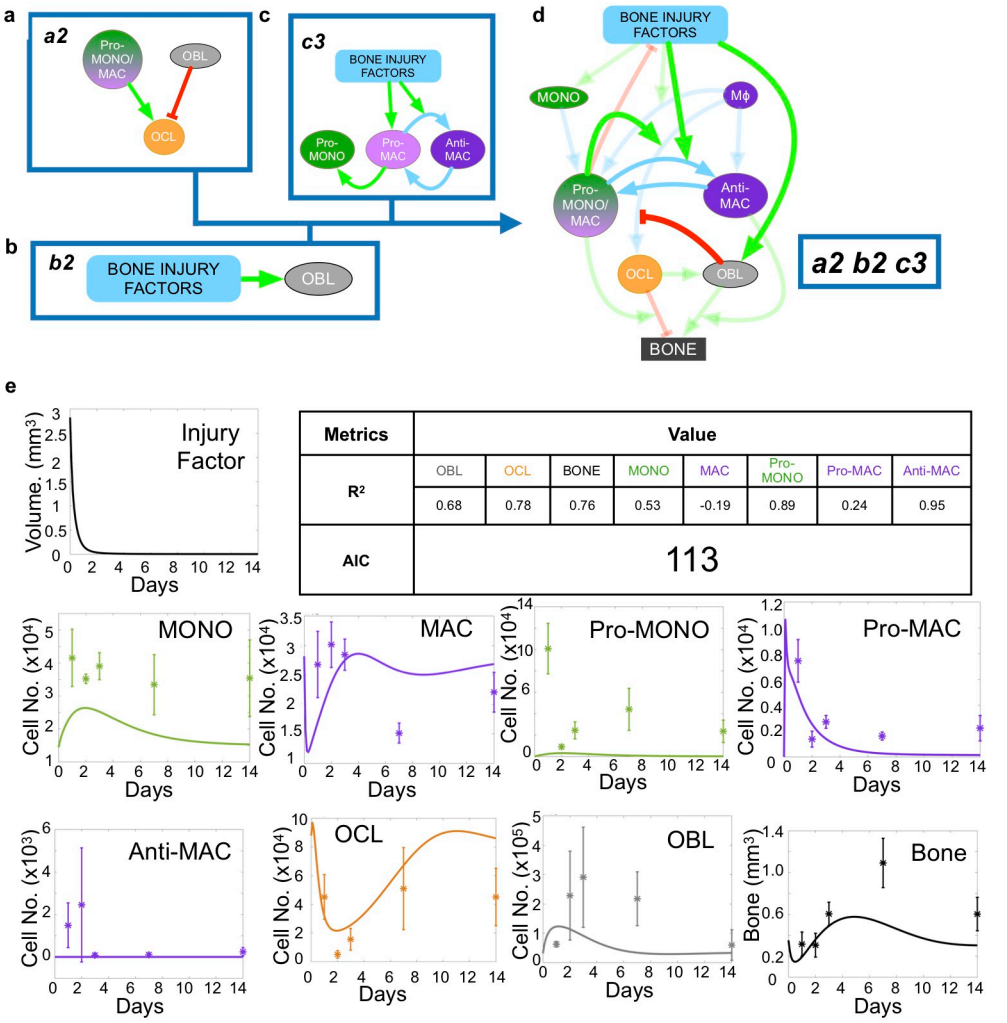

Fig 4. Other hypotheses combinations fail to recapitulate in vivo data. The example of the worst fitting hypothesis *a2-b2-c1* fails to recapitulate *in vivo* data. **a** mechanism *a2* assumes that pro-inflammatory monocytes/macrophages and osteoblasts promote and inhibit osteoclast formation, respectively. **b** mechanism *b2* assumes that injury factors promote osteoblast expansion. **c** mechanism *c1* assumes that injury factors promote pro-inflammatory monocytes/macrophages and anti-inflammatory macrophages polarization. Anti-inflammatory macrophages drive depolarization of monocytes/macrophages back to the naive state. **d** schematic representation of the model using *a2-b2-c1* hypothesis combination. Arrows represent positive (green) or negative (red) types of cellular interactions. **e** temporal plots and corresponding goodness of fit metrics (AIC and R2s) across all populations, obtained through J_∞ minimization.

https://doi.org/10.1371/journal.pcbi.1009839.g004

information as to the importance of key populations of cells, such as macrophages, but these approaches seldomly address the direct and indirect effects of other cell types involved in bone injury repair. Mathematical modeling has the advantage of being able to consider complex biological processes resulting from the interactions between several cellular populations, but their relevance is limited by the availability of biological parameters and validation data. Here, by combining experimental and mathematical models, we have investigated the interactions between cell populations in bone that synchronously orchestrate the bone injury repair program. To do so, we built a mathematical model that captures the dynamics of seven cell populations and the bone mass. Importantly, the system of equations is coupled so that each cell

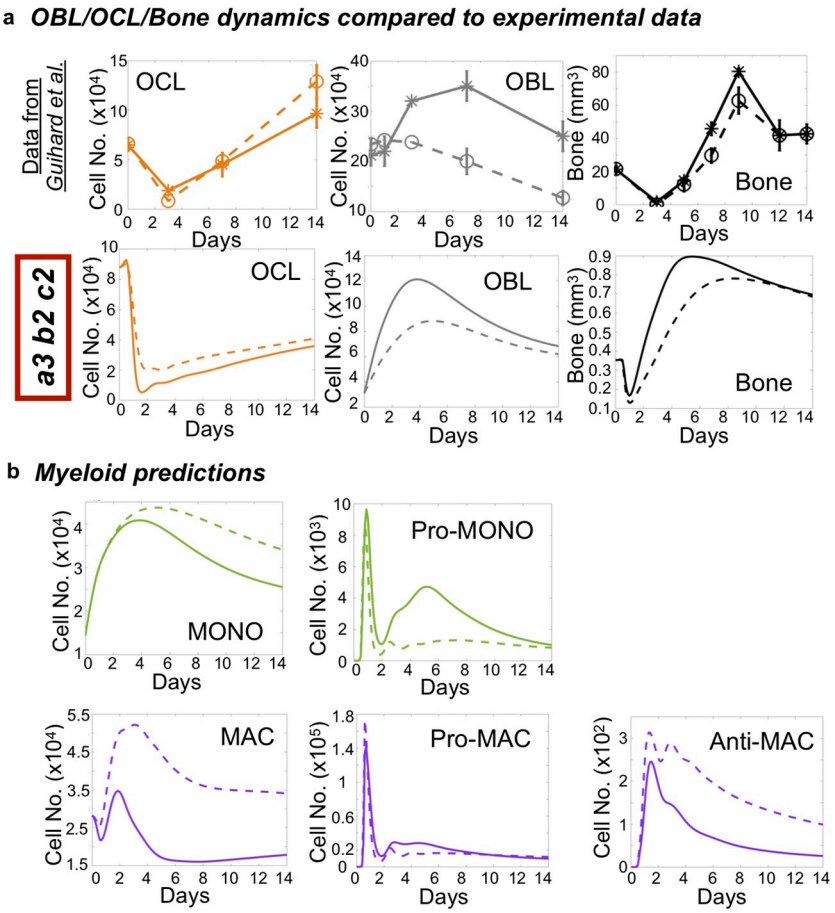

Fig 5. Bone repair dynamics in oncostatin M (OSM)-depleted bone predictions. a bone repair temporal data for OCL, OBL and bone, in presence or absence of OSM, is retrieved and plotted from a murine *in vivo* bone fracture healing study performed by *Guihard P*, *et al* [49]. on the top panel (solid line = WT, dashed line = OSM-null; http://doi.org/10.1016/j.ajpath.2014.11.008). Reduction in OBL bone formation rate and mineralization activity, allow model to qualitatively reproduce OBL, OCL and bone dynamics in OSM-null dataset (lower panel; solid line = unmodulated, dashed line = $OSM^{-/-}$). **b.** corresponding Myeloid populations predictions with reduced OBL formation rate and mineralization activity (lower panel; solid line = unmodulated, dashed line = $OSM^{-/-}$), for which no data was available in *Guihard P*, *et al* [49]. Simulations were obtained with model *a2-b2-c1*, calibrated on the injury data (Fig 4) through J_∞ minimization.

https://doi.org/10.1371/journal.pcbi.1009839.g005

type can regulate the activity of other cell types. This interplay between the different populations poses a challenge regarding the reconciliation between model dynamics and experimental data but gives credence to the novel insights it has allowed us to uncover. These include 1) Anti-inflammatory macrophages drive early osteoclast inhibition and pro-inflammatory phenotype suppression 2) pro-inflammatory macrophages are involved in osteoclast activation (bone resorptive activity), whereas osteoblastic cells promote osteoclast differentiation 3) Pro-inflammatory monocytes/macrophages rise during two expansion waves, which can be explained by the anti-inflammatory macrophages-mediated inhibition phase between the two waves.

Experimentally, as described in our previous study [40], we observe a rapid expansion of pro-inflammatory monocytes and macrophages in the first 24 hours with anti-inflammatory macrophages emerging shortly thereafter and persisting for up 48 hours. Of the hypotheses

tested by the model, *a3-b2-c2* provided the best fit of model simulations to experimental data. Under this set of assumptions, anti-inflammatory macrophages cause retraction of the pro-inflammatory population and facilitates osteoblast expansion and mineralization/stabilization of the injury site. With the natural depletion of the anti-inflammatory population, the remaining injury-associated factors causes a second expansion of pro-inflammatory macrophages and monocytes that in turn enhance osteoclast formation and activity. This increased activity is essential for the resorption of the mineralized callus at the site of injury and the return to bone homeostasis in the given time frame. To our knowledge very few reports have proposed a role and mechanism for this second inflammatory wave during bone healing. A role of MSCs and osteoblastic cells has been proposed for a second increase in inflammatory cytokines like TNF [56]. However, this two waves pattern has been observed in larger spectrum of inflammatory contexts, not only in bone [51,106–108], suggesting that this temporal profile is not bone specific. Importantly, to our knowledge the present study is the first to propose a mathematical framework of bone healing where bone and immune cell populations are fully coupled and to inform such a model with experimental longitudinal data of all these populations.

Our hypothesis combination approach allowed us to explore the polarization properties of monocytes/macrophages that can be difficult to determine *in vivo*. For example, the best fitting ODE model, *a3-b2-c2* allowed us to estimate the rates of pro- and anti-inflammatory macrophage polarization and indicates that pro-inflammatory macrophages do not re-polarize into an anti-inflammatory phenotype given the time frame, which goes against studies suggesting macrophage plasticity and reprogramming, at least in the context of bone injury repair. While not disputing the possibility that macrophages can repolarize, our results suggest that, based on the timing of the acquired experimental timing points, repolarization does not appear to be the main mechanism that recapitulates macrophage polarization dynamics. Additional insights provided by the ODE model include estimations on macrophage lifespan during the healing process and the contributory roles of pro-inflammatory macrophages and monocytes to the process. This information can be critical for therapies that target specific myeloid populations during bone injury repair in a bid to accelerate bone healing.

Another important result of our study is that the hypothesis combination that fit the best, *a3-b2-c2*, implies that osteoblast and pro-inflammatory monocytes-macrophages have distinct roles in osteoclast biology. According to this model, osteoblast drives osteoclast differentiation, whereas pro-inflammatory monocytes-macrophages drive osteoclast resorptive activity. In most studies, this distinction is not made and both cell types are assumed to contribute to both osteoclast differentiation and resorptive activity. The data we present here suggest a distinction in osteoclast supportive functions. This hypothesis combination has been also used to simulate OSM depletion bone injury process. Model simulations were in accordance with experimental data from an independent published study.

An important aspect of mathematical modeling is that it allows us to distill the key cell species and molecules driving the bone dynamics. Of note, our model does not consider the potential roles of other cell types in the bone ecosystem that could contribute, such as T cells. Our results suggest that that integrating myeloid populations into the model provides enough resolution to explain the process of non-critical bone injury repair. Our mathematical framework is flexible enough, however, that the effects of other immune cells such as T cells could be included. Additionally, we are aware the hypotheses we have identified throughout this study, while the most common, do not cover exhaustively all myeloid behaviors described in literature. However, the hypothesis testing pipeline we have devised enables us to efficiently adapt our model to reflect any additional hypotheses. Another important aspect that our model currently neglects is that of bone quality which requires a different set of data acquisition

techniques and further refinement of the mathematical approach. Moreover, bone healing is a spatially regulated process and having this aspect included in the model would be an exciting refinement in order to explore further mechanistic aspects of bone structure and regeneration.

Through our hypothesis combination approach, we have integrated established biology into a mathematical framework describing cell population dynamics during non-critical bone injury repair. One potential application of our framework is to investigate how time to healing subsequent to bone injury can be reduced. Existing studies have shown that bone healing times can be impacted in modulating pro- and anti-inflammatory macrophages [10,109,110,117]. While the model is parameterized with mouse data, there is much overlap between mice and humans with respect to the phases of the bone injury repair program. Thus, using our existing workflow, we can conceivably re-parameterize our model with human patient-derived data to further its potential as a relevant prospective tool for the clinic.

In conclusion, we have developed a coupled ordinary differential equation (ODE) system of the bone ecosystem that models the interplay between 8 key cellular populations during bone injury repair. The model yields several novel findings regarding macrophage dynamics and macrophage impact on osteoblasts and osteoclasts dynamics. Further, the model can also provide novel insights into phenomena that are hard to measure *in vivo* such as rate of pro- or anti-inflammatory polarization over time. A better understanding of bone healing will have clinical translatability allowing, for instance, to accelerate the process and improve patient outcomes. The model accounts for coupling between these population and will be useful in developing therapeutic strategies/interventions that shorten healing times. Further, the model has broad applicability and can be used as a platform to examine other bone diseases such as osteoarthritis and skeletal malignancies such as bone-metastatic cancer.

Materials and methods

Ethics statement

Data from in vivo bone injury experiment were derived from our previous work [40]. In this study, all animal studies were performed in accordance with Guidelines for the Care and Use of Laboratory Animals published by the National Institutes of Health, and approved by the Animal Care and Use Committee at the University of South Florida, under IACUC Protocol R5857 (CCL). Male C57BL/6 mice (5–6 weeks old) were purchased from Jackson Laboratory. Mice (n = 30) were subject to tibial bone injury by penetration of a 28-gauge (0.3062mm diameter) syringe through the knee epiphysis to mid-shaft.

Intratibial bone injury model

Data from in vivo bone injury experiment were derived from our previous work [40]. In this study, all animal studies were performed in accordance with Guidelines for the Care and Use of Laboratory Animals published by the National Institutes of Health, and approved by the Animal Care and Use Committee at the University of South Florida, under IACUC Protocol R5857 (CCL). Male C57BL/6 mice (5–6 weeks old) were purchased from Jackson Laboratory. Mice (n = 30) were subject to tibial bone injury by penetration of a 28-gauge (0.3062mm diameter) syringe through the knee epiphysis to mid-shaft. Mice tibias at baseline and at days 1, 2, 3, 7 and 14 (n = 5/time point) were collected for analysis. Temporal population data was used to parameterize subsequent mathematical models.

Micro-computed topography

Bone volume data was derived from formalin-fixed tibias by micro-computed topography (μCT) scanning using Scanco μ35 scanner. Endosteal trabecular bone volume was analyzed 100μm away from the tip of growth plate to clear the dense bone nature of the growth plate. 1000μm along the midshaft of each bone was then scanned and analyzed using built-in functions (n = 30 bones; 5/time point).

TRAcP staining

After μCT analysis, tibia bones were decalcified using 14% EDTA for 3 weeks for further staining quantitation and analyses. Decalcified bones were sectioned at 4μm thickness. Sections were enzymatically stained for tartrate-resistant acid phosphatase (TRAcP) for osteoclast numbers based on manufacturer's protocol [120]. Stained slides were imaged using the Evos Auto microscope to capture 20X photos which included injury site and its immediate periphery. All TRAcP positive (red) multinucleated osteoclasts within 5μm radius from injury were counted, and mathematically converted to osteoclasts / bone marrow volume (#OCL/μm^3) for each bone at each time point.

Immunofluorescence staining and quantitation

FFPE tibia bones were further sequentially sectioned and baked at 56˚C in preparation for immunofluorescence staining of osteoblast (RUNX2 at 1:500; Abcam Cat. No. ab81357) and nuclear staining (DAPI). Deparaffined and rehydrated slides were subject to heat-induced antigen retrieval method. Sections were then blocked and incubated in primary antibodies diluted in 10% normal goat serum in TBS overnight at 4˚C. Subsequently, slides were stained with secondary Alexa Fluor 568-conjugated antibody at 1:1000 at room temperature for 1 hour under light-proof conditions. Stained slides were stained with DAPI for nuclear contrast and mounted for imaging at 20X using Zeiss upright fluorescent microscope to include the injury site as well as the immediate peripheral tissue. All runx2 positive cells (red staining colocalizing with DAPI) within 5μm radius from injury were counted and mathematically converted to osteoblasts / bone marrow volume (#OBL/μm^3) for each bone at each time point.

Flow cytometry and analysis

Harvested contralateral injured tibias (n = 30; 5/time point) had tips removed and were subjected to centrifugation at 16,000g for 5 seconds for isolation of whole bone marrow for flow cytometry staining and analysis. Red blood cells were lysed using RBC Lysis Buffer from Sigma Aldrich (Cat. No. R7757-100ML) as per manufacturer's guidelines. Live bone marrow cells were subject to FcR-receptor blocking (1:3; BioLegend; Cat. No. 101319) and viability staining (1:500; BioLegend; Cat. No. 423105). Samples were then stained by cell-surface conjugated antibodies from BioLegend diluted in autoMACS buffer (Miltenyi; Cat. No. 130-091-221) for phenotyping myeloid cells: CD11b-BV786 (1:200; Cat. No. 101243), LY-6C-Alexa Fluor 488 (1:500; Cat. No.128021) and LY-6G-Alexa Fluor 700 (1:200; Cat. No. 561236). Cells were then fixed with 2% paraformaldehyde in dark prior to intracellular staining. Fixed cells were permeabilized using intracellular conjugated antibodies to assess polarization status: NOS2-APC (1:100; eBioscience; Cat. No. 17-5920-80) and ARG1-PE (1:100; R&D; Cat. No. IC5868P). Appropriate compensation and fluorescence-minus-one (FMO) controls were generated in parallel either with aliquots of bone marrow cells or Rainbow Fluorescent Particle beads (BD Biosciences; Cat. No. 556291). All antibody concentrations were titrated prior to injury study using primary bone marrow cells to ensure optimal separation and detection of true negative

and positive populations. Stained controls and samples were analyzed using BD Biosciences LSR flow cytometer (S2 Fig).

Mathematical and computational methods

Comprehensive model structure. In order to efficiently describe the process of model building regarding the different hypothesis combinations (Fig 2), we begin with a generic set of coupled equations, using a formulation that is valid for all hypotheses combinations (S3 Fig). For all populations, homeostasis was described by a replenishment term and a clearance term. For polarized monocytes/ macrophages, no replenishment was considered at homeostasis, as the baseline measured by flow cytometry was close to zero. Here is the detailed description, equation by equation:

Equation 1: Naive monocytes.

$$\frac{dMo}{dt} = H_{Mo} - \delta_{Mo}Mo + I(M_1 + Mo_1, D) - p_3(D, M_1, Mo_1)Mo + depol_3(M_2)Mo_1$$

Naive monocytes are assumed to be replenished at a constant rate H_{Mo}, and to die at a rate $\delta_{Mo}Mo$. δ_{Mo}, the lifespan parameter, was retrieved from literature (Table 4), and H_{Mo} was estimated so that monocyte level at homeostasis would match experimentally measured monocyte baseline. The term $I(M_1, Mo_1, D)$ corresponds to the number of monocytes infiltrating the bone marrow per unit of time due to injury factors and pro-inflammatory cells. It is equal to $I_1(M_1 + Mo_1) + I_2D$. As indicated by the mathematical formulation, inflammation-associated monocyte recruitment is driven by injury signals on one hand, and pro-inflammatory monocytes/macrophages on the other hand. This reflects the fact that cellular debris and pro-inflammatory cells produce factors that help recruiting additional monocytes [1]. The term $p_3(D, M_1, Mo_1)Mo$ represents the number of naive monocytes polarizing into pro-inflammatory monocytes per unit of time, as a function of cellular debris and pro-inflammatory cells. The term $depol_3(M_2)Mo_1$ represents the number pro-inflammatory monocytes reverting back to a naive state per unit of time, as function of anti-inflammatory macrophages.

Equation 2: Naive macrophages.

$$\begin{aligned}\frac{dM}{dt} = \quad & H_M - \delta_M M - d_{OC}(OB, M_1, Mo_1, M_2)M - p_1(D, M_1, Mo_1)M \\ & - p_{21}(D, M_1, Mo_1)M + depol_1(M_2)M_1 + depol_{21}M_2\end{aligned}$$

Naive macrophage are assumed to be replenished at a constant rate H_M, and to die at a rate $\delta_M M$. δ_M, the lifespan parameter, was retrieved from literature (Table 4), and H_M was estimated so that macrophage level at homeostasis would match experimentally measured macrophage baseline. The term $d_{OC}(OB, M_1, Mo_1, M_2)M$ corresponds to the number of macrophages differentiating into osteoclasts per unit of time, as a function of osteoblasts (RANKL, OPG), pro-inflammatory macrophages (IL-1, TNF), pro-inflammatory monocytes (IL-1, TNF) and anti-inflammatory macrophages (IL-10, TGF). The term $p_1(D, M_1, Mo_1)M$ represents the number of naive macrophages polarizing into a pro-inflammatory state per unit of time, as a function of injury factors and pro-inflammatory cells. The term $p_{21}(D, M_1, Mo_1)M$ represents the number of naive macrophages polarizing into an anti-inflammatory state per unit of time, as a function of injury factors and pro-inflammatory cells. The term $depol_1(M_2)M_1$ represents the number of pro-inflammatory macrophages that revert back to a naive state per unit of time, as a function of anti-inflammatory macrophages. The term $depol_{21}M_2$ represents the number of anti-inflammatory macrophages that

revert back to a naive state per unit of time. Of note, no influx or differentiation from monocytes during inflammation were assumed, as macrophage population does not show evidence of expansion in our obtained biological data.

Equation 3: Pro-inflammatory macrophages.

$$\frac{dM_1}{dt} = p_1(D, M_1, Mo_1)M - depol_1(M_2)M_1 - p_{22}(D)M_1 + depol_{22}M_2 - \delta_M M_1$$

Pro-inflammatory macrophages are assumed to be absent of the bone marrow under homeostatic conditions, as experimental al baseline level did not 0.3% across the replicates. The term $p_1(D, M_1, Mo_1)M$ represents the number of pro-inflammatory macrophages generated (from naive pool) per unit of time, as a function of injury factors and pro-inflammatory cells. The term $depol_1(M_2)M_1$ represents the number of pro-inflammatory macrophages that revert back to a naive state per unit of time, as a function of anti-inflammatory macrophages. The term $depol_{22}M_2$ represents the number of anti-inflammatory macrophages that reprogram into a pro-inflammatory phenotype. The term $p_{22}(D)M_1$ represents the number of pro-inflammatory macrophages that reprogram into an anti-inflammatory phenotype, as a function of injury factors.

Equation 4: Anti-inflammatory macrophages.

$$\frac{dM_2}{dt} = p_{21}(D, M_1, Mo_1)M + p_{22}(D)M_1 - depol_{21}M_2 - depol_{22}M_2 - \delta_M M_2$$

Anti-inflammatory macrophages are assumed to be absent of the bone marrow under homeostatic conditions, as experimental al baseline level did not exceed 0.07% across the replicates. The term $p_{21}(D, M_1, Mo_1)M$ represents the number of anti-inflammatory macrophages generated (from naive pool) per unit of time, as a function of injury factors and pro-inflammatory cells. The term $p_{22}(D)M_1$ represents the number of pro-inflammatory macrophages that reprogram into an anti-inflammatory phenotype, as a function of injury factors. The term $depol_{21}M_2$ represents the number of pro-inflammatory macrophages that revert back to a naive state per unit of time. The term $depol_{22}M_2$ represents the number of anti-inflammatory macrophages that reprogram into a pro-inflammatory phenotype.

Equation 5: Pro-inflammatory monocytes.

$$\frac{dMo_1}{dt} = p_3(D, M_1, Mo_1)Mo - depol_3(M_2)Mo_1 - \delta_{Mo}Mo_1$$

Pro-inflammatory monocytes are assumed to be absent of the bone marrow under homeostatic conditions, as experimental al baseline level did not exceed 0.16% across the replicates. The term $p_3(D, M_1, Mo_1)Mo$ represents the number of pro-inflammatory monocytes generated (from naive pool) per unit of time, as a function of injury factors and pro-inflammatory cells. The term $depol_3(M_2)Mo_1$ represents the number of pro-inflammatory monocytes that revert back to a naive state per unit of time, as a function of anti-inflammatory macrophages. The term $depol_{22}M_2$ represents the number of anti-inflammatory macrophages that reprogram into a pro-inflammatory phenotype. The term $p_{22}(D)M_1$ represents the number of pro-inflammatory macrophages that reprogram into an anti-inflammatory phenotype, as a function of injury factors.

Pro-inflammatory macrophages/monocytes and anti-inflammatory macrophages: Hypothesis c1.

$$p_1(D, M_1, Mo_1) = p_{11}D + p_{12}D(M_1 + Mo_1)$$
$$depol_1(M_2) = depol_1 M_2$$
$$p_{21}(D, M_1, Mo_1) = 0$$
$$p_{22}(D) = p_2 D$$
$$depol_{21} = depol_2$$
$$depol_{22} = 0$$
$$p_3(D, M_1, Mo_1) = p_{31}D + p_{32}D(M_1 + Mo_1)$$
$$depol_3(M_2) = depol_3 M_2$$

Both CD11b+Ly6C+ monocytes and CD11b+Ly6C- macrophages can polarize into a pro-inflammatory phenotype [1], in response to injury signals or to factors produced by already present pro-inflammatory cells [1]. In assumptions c1 and c2, monocytes and macrophages polarize into pro-inflammatory monocytes and macrophages respectively through two terms. The first is proportional to the amount of injury signals present and the second is proportional to the amount of pro-inflammatory cells present. In the assumption c3, injury signals polarize local resident macrophages, and those in turn promote polarization of pro-inflammatory monocytes. In c3, pro-inflammatory macrophages repolarize into anti-inflammatory macrophages by the uptake of cellular debris/injury signals [121]. In this scenario, by plasticity, anti-inflammatory macrophages naturally return to a pro-inflammatory phenotype in absence of signals [122]. Polarization into anti-inflammatory macrophages was assumed to be proportional to the amount of injury signals for assumption c1, proportional to the amount of pro-inflammatory cells for assumption c2, and a transition term from pro-inflammatory macrophages for c3.

Pro-inflammatory macrophages/monocytes and anti-inflammatory macrophages: Hypothesis c2.

$$p_1(D, M_1, Mo_1) = p_{11}D + p_{12}D(M_1 + Mo_1)$$
$$depol_1(M_2) = depol_1 M_2$$
$$p_{21}(D, M_1, Mo_1) = p_2(M_1 + Mo_1)$$
$$p_{22}(D) = 0$$
$$depol_{21} = depol_2$$
$$depol_{22} = 0$$
$$p_3(D, M_1, Mo_1) = p_{31}D + p_{32}D(M_1 + Mo_1)$$
$$depol_3(M_2) = depol_3 M_2$$

Both CD11b+Ly6C+ monocytes and CD11b+Ly6C- macrophages can polarize into a pro-inflammatory phenotype [1], in response to injury signals or to factors produced by already present pro-inflammatory cells [1]. In assumptions c1 and c2, monocytes and macrophages polarize into pro-inflammatory monocytes and macrophages respectively through two terms. The first is proportional to the amount of injury signals present and the second is proportional to the amount of pro-inflammatory cells present. In the assumption c3, injury signals polarize local resident macrophages, and those in turn promote polarization of pro-inflammatory monocytes. In c3, pro-inflammatory macrophages repolarize into anti-inflammatory

macrophages by the uptake of cellular debris/injury signals [121]. In this scenario, by plasticity, anti-inflammatory macrophages naturally return to a pro-inflammatory phenotype in absence of signals [122]. Polarization into anti-inflammatory macrophages was assumed to be proportional to the amount of injury signals for assumption c1, proportional to the amount of pro-inflammatory cells for assumption c2, and a transition term from pro-inflammatory macrophages for c3.

Pro-inflammatory Macrophages/Monocytes and Anti-inflammatory Macrophages: Hypothesis c3.

$$p_1(D, M_1, Mo_1) = p_{11}D$$
$$depol_1(M_2) = 0$$
$$p_{21}(D, M_1, Mo_1) = 0$$
$$p_{22}(D) = p_2 D$$
$$depol_{21} = 0$$
$$depol_{22} = depol_2$$
$$p_3(D, M_1, Mo_1) = p_{32}M_1$$
$$depol_3(M_2) = depol_3$$

Both CD11b+Ly6C+ monocytes and CD11b+Ly6C- macrophages can polarize into a pro-inflammatory phenotype [1], in response to injury signals or to factors produced by already present pro-inflammatory cells [1]. In assumptions c1 and c2, monocytes and macrophages polarize into pro-inflammatory monocytes and macrophages respectively through two terms. The first is proportional to the amount of injury signals present and the second is proportional to the amount of pro-inflammatory cells present. In the assumption c3, injury signals polarize local resident macrophages, and those in turn promote polarization of pro-inflammatory monocytes. In c3, pro-inflammatory macrophages repolarize into anti-inflammatory macrophages by the uptake of cellular debris/injury signals [121]. In this scenario, by plasticity, anti-inflammatory macrophages naturally return to a pro-inflammatory phenotype in absence of signals [122]. Polarization into anti-inflammatory macrophages was assumed to be proportional to the amount of injury signals for assumption c1, proportional to the amount of pro-inflammatory cells for assumption c2, and a transition term from pro-inflammatory macrophages for c3.

Equation 6: Osteoblasts.

$$\frac{dOB}{dt} = H_{OB}OC + \gamma_{OB}(D, M_2) - \delta_{OB}OBB$$

Osteoblast are assumed to be replenished at a rate $H_{OB}OC$, proportional to osteoclasts. This reflects the ability of osteoclasts to produce osteogenic signals like transforming growth factor β (TGFβ) and bone morphogenetic proteins (BMPs) [123]. Similar assumptions are considered in published works of homeostatic bone remodeling [32–34]. Osteoblasts are assumed to die at a rate $\delta_{OB}OBB$. δ_{OB}, the lifespan parameter, was retrieved from literature (Table 4), and H_{OB} was estimated so that osteoblast level at homeostasis would match experimentally measured osteoblast baseline. The term $\gamma_{OB}(D, M_2)$ represents the number of osteoblasts generated per unit of time, as a function of injury factors and anti-inflammatory factors.

Osteoblast dynamics: Hypothesis b1.

$$\gamma_{OB}(D, M_2) = \gamma_{OB}M_2$$

The osteoblast clearance term was assumed to be proportional to the bone volume, in order to account for osteoblast differentiation into osteocytes, when resorbing bone matrix [123]. A similar assumption is made in the model developed by Ryser et al. that describes bone remodeling as a spatial evolutionary game [124]. During injury, an extra term for osteoblast expansion is present, driven by anti-inflammatory macrophages (hypothesis b1) or injury factors (hypothesis b2), both supported by literature [1,3,6,7,125].

Osteoblast dynamics: Hypothesis b2.

$$\gamma_{OB}(D, M_2) = \gamma_{OB} D$$

The osteoblast clearance term was assumed to be proportional to the bone volume, in order to account for osteoblast differentiation into osteocytes, when resorbing bone matrix [123]. A similar assumption is made in the model developed by Ryser et al. that describes bone remodeling as a spatial evolutionary game [124]. During injury, an extra term for osteoblast expansion is present, driven by anti-inflammatory macrophages (hypothesis b1) or injury factors (hypothesis b2), both supported by literature [1,3,6,7,125].

Equation 7: Osteoclasts.

$$\frac{dOC}{dt} = d_{OC}(OB, M_1, Mo_1, M_2)M - \delta_{OC}(M_2, OB)OC$$

Osteoclasts are assumed to be replenished at a rate $d_{OC}(OB, M_1, Mo_1, M_2)M$, which reflects differentiation of macrophages into osteoclasts, as a function of osteoblasts, pro-inflammatory macrophages, pro-inflammatory monocytes, anti-inflammatory macrophages [126–128]. This reflects osteoclastic factors produced by osteoblasts (RANKL) and pro-inflammatory monocytes/macrophages (IL-1, TNF), as well as anti-osteoclastic factors produced by osteoblasts (OPG) and anti-inflammatory macrophages (transforming growth factor β (TGFβ), IL-10). The term $\delta_{OC}(M_2, OB)OC$ represents the number of osteoclasts dying per unit of time, as a function of anti-inflammatory macrophages and osteoblasts. This reflects factors produced by anti-inflammatory macrophages (IL-10, TGFβ) and osteoblasts (OPG) that reduce osteoclast lifespan.

Osteoclast dynamics: Hypothesis a1.

$$d_{OC}(OB, M_1, Mo_1, M_2) = \frac{d_{OC} + d_{OC2}(M_1 + Mo_1)}{1 + Inhib_{OC} M_2}$$

$$\delta_{OC}(M_2, OB) = \delta_{OC}(1 + Inhib_{OC2} M_2)$$

This osteoclast formation term was assumed to be proportional to osteoblasts for assumption a3, reflecting the ability of osteoblastic cells to produce RANKL, which is an essential mediator of osteoclast formation [123]. For the other assumptions, homeostatic osteoclast replenishment was assumed to be constant. This term had an additional contribution from pro-inflammatory monocytes/macrophages for assumptions a1 and a2, representing the ability of pro-inflammatory monocytes/macrophages to produce factors like IL-1 and TNF that favor osteoclast formation [123,129]. Osteoclast formation was divided by an inhibitory term, a linear function of anti-inflammatory macrophages for assumptions a1 and a3, and a linear function of osteoblasts for assumption a2. The first assumption reflects factors produced by anti-inflammatory macrophages, like IL-10, that disrupt osteoclast formation [86], whereas the second reflects the ability of osteoblasts to produce osteoprotegerin (OPG), a RANKL decoy receptor [123]. Moreover, this inhibition affects not only the ability of monocytes-macrophages to fuse and form osteoclasts, but also their life span. Indeed RANKL is necessary for osteoclast survival

since OPG produced by osteoblasts reduces their life span [130]. Similarly, anti-inflammatory macrophages produce TGFβ, which is known to drive osteoclast apoptosis [131].

Osteoclast dynamics: Hypothesis a2.

$$d_{OC}(OB, M_1, Mo_1, M_2) = \frac{d_{OC} + d_{OC2}(M_1 + Mo_1)}{1 + Inhib_{OC}OB}$$
$$\delta_{OC}(M_2, OB) = \delta_{OC}(1 + Inhib_{OC2}OB)$$

This osteoclast formation term was assumed to be proportional to osteoblasts for assumption a3, reflecting the ability of osteoblastic cells to produce RANKL, which is an essential mediator of osteoclast formation [123]. For the other assumptions, homeostatic osteoclast replenishment was assumed to be constant. This term had an additional contribution from pro-inflammatory monocytes/macrophages for assumptions a1 and a2, representing the ability of pro-inflammatory monocytes/macrophages to produce factors like IL-1 and TNF that favor osteoclast formation [123,129]. Osteoclast formation was divided by an inhibitory term, a linear function of anti-inflammatory macrophages for assumptions a1 and a3, and a linear function of osteoblasts for assumption a2. The first assumption reflects factors produced by anti-inflammatory macrophages, like IL-10, that disrupt osteoclast formation [86], whereas the second reflects the ability of osteoblasts to produce osteoprotegerin (OPG), a RANKL decoy receptor [123]. Moreover, this inhibition affects not only the ability of monocytes-macrophages to fuse and form osteoclasts, but also their life span. Indeed RANKL is necessary for osteoclast survival since OPG produced by osteoblasts reduces their life span [130]. Similarly, anti-inflammatory macrophages produce TGFβ, which is known to drive osteoclast apoptosis [131].

Osteoclast dynamics: Hypothesis a3.

$$d_{OC}(OB, M_1, Mo_1, M_2) = \frac{d_{OC}OB}{1 + Inhib_{OC}M_2}$$
$$\delta_{OC}(M_2, OB) = \delta_{OC}(1 + Inhib_{OC2}M_2)$$

This osteoclast formation term was assumed to be proportional to osteoblasts for assumption a3, reflecting the ability of osteoblastic cells to produce RANKL, which is an essential mediator of osteoclast formation [123]. For the other assumptions, homeostatic osteoclast replenishment was assumed to be constant. This term had an additional contribution from pro-inflammatory monocytes/macrophages for assumptions a1 and a2, representing the ability of pro-inflammatory monocytes/macrophages to produce factors like IL-1 and TNF that favor osteoclast formation [123,129]. Osteoclast formation was divided by an inhibitory term, a linear function of anti-inflammatory macrophages for assumptions a1 and a3, and a linear function of osteoblasts for assumption a2. The first assumption reflects factors produced by anti-inflammatory macrophages, like IL-10, that disrupt osteoclast formation [86], whereas the second reflects the ability of osteoblasts to produce osteoprotegerin (OPG), a RANKL decoy receptor [123]. Moreover, this inhibition affects not only the ability of monocytes-macrophages to fuse and form osteoclasts, but also their life span. Indeed RANKL is necessary for osteoclast survival since OPG produced by osteoblasts reduces their life span [130]. Similarly, anti-inflammatory macrophages produce TGFβ, which is known to drive osteoclast apoptosis [131].

Equation 8: Bone volume.

$$\frac{dB}{dt} = \Pi_B(1 + \beta M_2)OB - \delta_B(1 + \alpha(M_1 + Mo_1))OCB$$

Bone dynamics is described by two terms: a bone resorption term, which is the volume of bone resorbed per unit of time and is assumed to be proportional to the number of osteoclasts,

and a bone formation term, which is the volume of bone formed per unit of time and is assumed to be proportional to the number of osteoblasts. Such assumptions have been broadly used across a large variety of modeling studies [32–34]. $\delta_B(1+\alpha)OCB$ is the bone resorption term and is the sum of the two terms $\delta_B OCB$ (homeostatic resorption) and $\alpha(M_1 + Mo_1)\delta_B OCB$ (pro-inflammatory monocyte/macrophage mediated resorption). As indicated by this mathematical formulation, bone resorption was assumed to also be proportional to the bone mass. This reflects the fact that more bone volume increases the likelihood for bone resorption. Furthermore, this formulation ensures bone mass stays strictly positive in the model. $\Pi_B(1+\beta)OB$ is the bone formation term and is the sum of the two terms $\Pi_B OB$ (homeostatic bone formation) and $\beta M_2 \Pi_B OB$ (anti-inflammatory macrophage mediated bone formation). Under homeostasis, bone is formed at rate $\Pi_B OB$ and resorbed at rate $\delta_B OCB$. Resorption rate δ_B, as well as as parameters α and β, were calibrated on bone volume dynamics, and bone formation rate Π_B was then imposed by the relation $\Pi_B OB_0 = \delta_B OC_0 B_0$, which ensures that bone volume remains at homeostasis when osteoblasts and osteoclasts are at homeostatic levels. As indicated by mathematical formulations, bone formation and resorption terms were assumed to linearly increase with respect to anti-inflammatory and pro-inflammatory monocytes/ macrophages, respectively. This accounts for the fact that anti-inflammatory macrophages typically produce osteogenic factors like TGFβ or OSM, that are known to promote osteoblast expansion and bone mineralization [3], and for the fact that pro-inflammatory monocytes/macrophages typically produce osteolytic factors like TNF and IL-1, that are known to promote osteoclast resorptive activity [132].

Equation 9: Injury factors.

$$\frac{dD}{dt} = -\delta_D(M_1 + Mo_1)D$$

Injury factors dynamics consists in an exponential type of decay, with a decay rate δ_D $(M_1 + Mo_1)$ proportional to pro-inflammatory monocytes/macrophages number, which represents how pro-inflammatory monocytes/macrophages uptake cellular debris, which in return reduces pro-inflammatory signals.

Population homeostasis. In order to estimate the homeostatic cell replenishment parameters, we set them equal to the clearance term (lifespan) which was either based on literature values or calibrated directly from experimental data (S1 Fig and Tables 1, 4 and 5).

ODE solver. The ODE45 function of Matlab was used to solve the differential equation system. The experimental baseline values (time 0) were used as initial conditions.

Parameter estimation method. To estimate parameters for goodness of fit, we defined the following objective function:

$$J_2(\alpha) = \max_{1\le j\le 8} \sum_i^N \frac{\left(f_j(t_i,\alpha) - D_{ij}\right)^2}{\sigma_i^2}$$

$$J_\infty(\alpha) = \max_{1\le j\le 8} \max_{1\le i\le N} \frac{\left(f_j(t_i,\alpha) - D_{ij}\right)^2}{\sigma_i^2}$$

Where i represents the time point index and j the variable index, α represents the parameter set used to evaluate the model function f, D_{ij} represents the experimental data of variable j at time point i, σ_i represents the experimental standard deviation (over all the animals of a given time point), and N represents the number of time points. The functional J_2 corresponds to the weighted least squares criterion. The functional J_∞ is the Tchebychev approximation, which considers the maximal residual instead of the sum of the residuals. In both cases, the choice of

Table 5. Model variables description. Residuals lower than one for Mathematical model of all 18 combinations of hypotheses, resulting from J_2 and J_∞ minimization. For each hypothesis combination, the table shows how many residuals are lesser than 1 over all 40 residuals, which equates how many times the model lies within the experimental error bar.

Mathematical variable	Biological variable	Initial conditions	Units
OB	Osteoblasts	3,1×10^+04	Cell number
OC	Osteoclasts	8,8×10^+04	Cell number
B	Bone	0,3530	mm^3
D	Cellular debris/Injury factors	2,8	mm^3
Mo	Naive monocytes	1,4×10^+04	Cell number
M	Naive macrophages	2,8×10^+04	Cell number
M1	Pro-inflammatory macrophages	0	Cell number
M2	Anti-inflammatory macrophages	0	Cell number
Mo1	Pro-inflammatory monocytes	0	Cell number

https://doi.org/10.1371/journal.pcbi.1009839.t005

the max over the observed variables of the sum of the squares of the residuals was motivated to make sure that every variable was fitted with equal relative importance. Indeed, in the case of the minimization of the sum of the squares over all the variables, it is sometimes possible to find an optimum in minimizing certain variables at the detriment of others. This way, we ensure that all variables are equally well fitted.

The reason for considering the objective function J_∞ in addition to the classical criterion J_2 is to avoid neglecting any time point in the fit. The least squares functional allows sometimes to find an optimum optimizing certain time points at the detriment of others. In this current study, this is a potentially big issue, as the time sampling is not homogenous across the time points, meaning that biological dynamics of importance might be ignored, while still producing a good fit under the least squares metric.

In order to minimize this function representing the error estimate between data and model, we used the Matlab function fminsearch with a penalization term to stay in a parameter range set with reasonable boundaries.

In order to rank the models in term of goodness of fit, we used AIC, that is defined as follows:

$$AIC(\alpha) = 2p + 2J(\alpha)$$

where p is the number of parameters, and the functional J is either J_2 or J_∞.

OSM knockout data. In order to retrieve data from the OSM knockout independent dataset, we used webplotdigitizer to collect datapoint from the plot presented in Guihard et al [49].

Supporting information

S1 Fig. ODE equations for the best fitting model: Hypothesis combination a3b2c2 The ODE systems govern behaviors of each population and are parameterized by published values when available, such as the natural lifespan of monocytes (δ_{Mo} in dMo/dt). Parameters with no reference publication were estimated to obtain best possible fits to temporal dynamics data (parameters in red) and are listed in Table 3. In all equations, black terms correspond to homeostatic dynamics, whereas red terms correspond to injury dynamics.
(TIFF)

S2 Fig. Alternative hypotheses combination a3 b1 c2 (green boxes in a-c) computational results. a Mechanism a3 assumes that osteoblasts and anti-inflammatory macrophages promote and inhibit osteoclast formation, respectively. b Mechanism b1 assumes that anti-

inflammatory macrophages promote osteoblast expansion. c Mechanism c2 assumes that injury factors promote pro-inflammatory monocytes/macrophages polarization. Pro-inflammatory monocytes/macrophages promote anti-inflammatory macrophages polarization, which in return drive depolarization of pro-inflammatory monocytes/macrophages back to the naive state. d Schematic representation of the model using a3b1c2 hypothesis combination. Arrows represent positive (green) or negative (red) types of cellular interactions. e Temporal plots and corresponding goodness of fit metrics (AIC and R2s) across all populations, obtained through J∞ minimization.
(TIFF)

S3 Fig. Generic formulation of coupled ODE models, valid for all hypotheses combinations. Each term (e.g formation rate, clearance, transition) is a functional form of other variables reflecting cellular interactions described in Fig 2. Black terms correspond to homeostasis, red terms correspond to injury dynamics and are described in details in Mathematical and Computational Methods.
(TIFF)

S4 Fig. Alternative hypotheses combination a3 b2 c1 (green boxes in a-c) computational results. a Mechanism a3 assumes that osteoblasts and anti-inflammatory macrophages promote and inhibit osteoclast formation, respectively. b Mechanism b2 assumes that injury factors promote osteoblast expansion. c Mechanism c1 assumes that injury factors promote pro-inflammatory monocytes/macrophages and anti-inflammatory macrophages polarization. Anti-inflammatory macrophages drive depolarization of pro-inflammatory monocytes/macrophages back to the naive state. d Schematic representation of the model using a3b2c1 hypothesis combination. Arrows represent positive (green) or negative (red) types of cellular interactions. e Temporal plots and corresponding goodness of fit metrics (AIC and R2s) across all populations, obtained through J∞ minimization.
(TIFF)

S5 Fig. Alternative hypotheses combination a3 b1 c1 (green boxes in a-c) computational results. a Mechanism a3 assumes that osteoblasts and anti-inflammatory macrophages promote and inhibit osteoclast formation, respectively. b Mechanism b21assumes that injury factors promote osteoblast expansion. c Mechanism c1 assumes that anti-inflammatory macrophages promote pro-inflammatory monocytes/macrophages and anti-inflammatory macrophages polarization. Anti-inflammatory macrophages drive depolarization of pro-inflammatory monocytes/macrophages back to the naive state. d Schematic representation of the model using a3b2c1 hypothesis combination. Arrows represent positive (green) or negative (red) types of cellular interactions. e Temporal plots and corresponding goodness of fit metrics (AIC and R2s) across all populations, obtained through J∞ minimization.
(TIFF)

S6 Fig. Alternative hypotheses combination a2 b1 c1 (green boxes in a-c) produces the second worst fit of all hypotheses combinations. a Mechanism a2 assumes that pro-inflammatory and macrophages and osteoblasts promote and inhibit osteoclast formation, respectively. b Mechanism b1 assumes that anti-inflammatory macrophages promote osteoblast expansion. c Mechanism c1 assumes that injury factors promote pro-inflammatory monocytes/macrophages polarization and anti-inflammatory macrophages. The latter drive depolarization of pro-inflammatory monocytes/macrophages back to the naive state. d Schematic representation of the model using a2b1c1 hypothesis combination. Arrows represent positive (green) or negative

(red) types of cellular interactions. e Temporal plots and corresponding goodness of fit metrics (AIC and R2s) across all populations, obtained through J∞ minimization.
(TIFF)

Author Contributions

Conceptualization: Etienne Baratchart, Chen Hao Lo, Conor C. Lynch, David Basanta.

Data curation: Etienne Baratchart, Chen Hao Lo.

Formal analysis: Etienne Baratchart, Chen Hao Lo.

Funding acquisition: Conor C. Lynch, David Basanta.

Investigation: Etienne Baratchart, Chen Hao Lo, Conor C. Lynch, David Basanta.

Methodology: Etienne Baratchart, Chen Hao Lo, Conor C. Lynch, David Basanta.

Project administration: Conor C. Lynch, David Basanta.

Software: Etienne Baratchart.

Supervision: Conor C. Lynch, David Basanta.

Validation: Etienne Baratchart, Chen Hao Lo.

Visualization: Etienne Baratchart, Chen Hao Lo.

Writing – original draft: Etienne Baratchart, Chen Hao Lo, Conor C. Lynch, David Basanta.

Writing – review & editing: Etienne Baratchart, Chen Hao Lo, Conor C. Lynch, David Basanta.

References

1. Schindeler A., McDonald M.M., Bokko P., Little D.G. Bone remodeling during fracture repair: The cellular picture. Semin Cell Dev Biol. 2008; 19, 459–466. https://doi.org/10.1016/j.semcdb.2008.07.004 PMID: 18692584
2. Mantovani A., Biswas S.K., Galdiero M.R., Sica A. & Locati M. Macrophage plasticity and polarization in tissue repair and remodelling. The Journal of pathology. 2013, 229, 176–185. https://doi.org/10.1002/path.4133 PMID: 23096265
3. Chang M.K, Raggatt L.J, Alexander K.A, Kuliwaba J.S, Fazzalari N.L, Schroder K, et al. Osteal tissue macrophages are intercalated throughout human and mouse bone lining tissues and regulate osteoblast function in vitro and in vivo. J Immunol. 2008, 181, 1232–1244. https://doi.org/10.4049/jimmunol.181.2.1232 PMID: 18606677
4. Alexander K.A, Chang M.K, Maylin E.R, Kohler T, Müller R, Wu A.C, et al. Osteal macrophages promote in vivo intramembranous bone healing in a mouse tibial injury model. Journal of bone and mineral research: the official journal of the American Society for Bone and Mineral Research. 2011, 26, 1517–1532.
5. Cho D.-I, Kim M.R, Jeong H.-y, Jeong H.C, Jeong M.H, Yoon S.H et al. Mesenchymal stem cells reciprocally regulate the M1/M2 balance in mouse bone marrow-derived macrophages. Exp Mol Med. 2014, 46, e70. https://doi.org/10.1038/emm.2013.135 PMID: 24406319
6. Loi F, Cordova L.A, Pajarinen J, Lin T-h, Yao Z, Goodman S.B et al. Inflammation, fracture and bone repair. Bone. 2016, 86, 119–130. https://doi.org/10.1016/j.bone.2016.02.020 PMID: 26946132
7. Horwood N.J. Macrophage Polarization and Bone Formation: A review. Clin Rev Allergy Immunol. 2016, 51, 79–86. https://doi.org/10.1007/s12016-015-8519-2 PMID: 26498771
8. Cho S.W, Soki F.N, Koh A.J, Eber M.R, Entezami P, Park S.I et al. Osteal macrophages support physiologic skeletal remodeling and anabolic actions of parathyroid hormone in bone. Proceedings of the National Academy of Sciences of the United States of America. 2014, 111, 1545–1550. https://doi.org/10.1073/pnas.1315153111 PMID: 24406853
9. Raggatt L.J, Wullschleger M.E, Alexander K.A, Wu A.C, Millard S.M, Kaur S et al. Fracture healing via periosteal callus formation requires macrophages for both initiation and progression of early

endochondral ossification. Am J Pathol. 2014, 184, 3192–3204. https://doi.org/10.1016/j.ajpath.2014.08.017 PMID: 25285719

10. Schlundt C, El Khassawna T, Serra A, Dienelt A, Wendler S, Schell H, et al. Macrophages in bone fracture healing: Their essential role in endochondral ossification. Bone. 2018; 106:78–89. Epub 2015/11/04. https://doi.org/10.1016/j.bone.2015.10.019 PMID: 26529389.
11. Wu, A.C., Raggatt, L.J., Alexander, K.A. & Pettit, A.R. Unraveling macrophage contributions to bone repair. Bonekey. 2013, Rep 2, 373.
12. Chan JK, Glass GE, Ersek A, Freidin A, Williams GA, Gowers K, et al. Low-dose TNF augments fracture healing in normal and osteoporotic bone by up-regulating the innate immune response. EMBO Mol Med. 2015; 7(5):547–61. Epub 2015/03/17. https://doi.org/10.15252/emmm.201404487 PMID: 25770819
13. Basanta D, Gatenby RA, Anderson AR. Exploiting evolution to treat drug resistance: combination therapy and the double bind. Mol Pharm. 2012; 9(4):914–21. Epub 2012/03/01. https://doi.org/10.1021/mp200458e PMID: 22369188
14. Eikenberry SE, Nagy JD, Kuang Y. The evolutionary impact of androgen levels on prostate cancer in a multi-scale mathematical model. Biol Direct. 2010; 5:24. Epub 2010/04/22. https://doi.org/10.1186/1745-6150-5-24 PMID: 20406442
15. Gatenby RA, Silva AS, Gillies RJ, Frieden BR. Adaptive therapy. Cancer Res. 2009; 69(11):4894–903. Epub 2009/06/03. https://doi.org/10.1158/0008-5472.CAN-08-3658 PMID: 19487300
16. Horn M, Glauche I, Muller MC, Hehlmann R, Hochhaus A, Loeffler M, et al. Model-based decision rules reduce the risk of molecular relapse after cessation of tyrosine kinase inhibitor therapy in chronic myeloid leukemia. Blood. 2013; 121(2):378–84. Epub 2012/11/24. https://doi.org/10.1182/blood-2012-07-441956 PMID: 23175686.
17. Leder K, Pitter K, LaPlant Q, Hambardzumyan D, Ross BD, Chan TA, et al. Mathematical modeling of PDGF-driven glioblastoma reveals optimized radiation dosing schedules. Cell. 2014; 156(3):603–16. Epub 2014/02/04. https://doi.org/10.1016/j.cell.2013.12.029 PMID: 24485463
18. Rockne R, Alvord EC Jr., Rockhill JK, Swanson KR. A mathematical model for brain tumor response to radiation therapy. J Math Biol. 2009; 58(4–5):561–78. Epub 2008/09/26. https://doi.org/10.1007/s00285-008-0219-6 PMID: 18815786
19. Swanson KR, Rockne RC, Claridge J, Chaplain MA, Alvord EC Jr., Anderson AR. Quantifying the role of angiogenesis in malignant progression of gliomas: in silico modeling integrates imaging and histology. Cancer Res. 2011; 71(24):7366–75. Epub 2011/09/09. https://doi.org/10.1158/0008-5472.CAN-11-1399 PMID: 21900399
20. Swanson KR, Rostomily RC, Alvord EC Jr. A mathematical modelling tool for predicting survival of individual patients following resection of glioblastoma: a proof of principle. Br J Cancer. 2008; 98(1):113–9. Epub 2007/12/07. https://doi.org/10.1038/sj.bjc.6604125 PMID: 18059395
21. Anderson AR, Quaranta V. Integrative mathematical oncology. Nat Rev Cancer. 2008; 8(3):227–34. Epub 2008/02/15. https://doi.org/10.1038/nrc2329 PMID: 18273038.
22. Araujo A, Cook LM, Lynch CC, Basanta D. An integrated computational model of the bone microenvironment in bone-metastatic prostate cancer. Cancer Res. 2014; 74(9):2391–401. Epub 2014/05/03. https://doi.org/10.1158/0008-5472.CAN-13-2652 PMID: 24788098
23. Anderson AR, Weaver AM, Cummings PT, Quaranta V. Tumor morphology and phenotypic evolution driven by selective pressure from the microenvironment. Cell. 2006; 127(5):905–15. Epub 2006/11/30. https://doi.org/10.1016/j.cell.2006.09.042 PMID: 17129778.
24. Benzekry S, Beheshti A, Hahnfeldt P, Hlatky L. Capturing the Driving Role of Tumor-Host Crosstalk in a Dynamical Model of Tumor Growth. Bio Protoc. 2015; 5(21). Epub 2016/07/28. https://doi.org/10.21769/bioprotoc.1644 PMID: 27453916
25. Benzekry S, Lamont C, Barbolosi D, Hlatky L, Hahnfeldt P. Mathematical Modeling of Tumor-Tumor Distant Interactions Supports a Systemic Control of Tumor Growth. Cancer Res. 2017; 77(18):5183–93. Epub 2017/07/22. https://doi.org/10.1158/0008-5472.CAN-17-0564 PMID: 28729417
26. Benzekry S, Lamont C, Beheshti A, Tracz A, Ebos JM, Hlatky L, et al. Classical mathematical models for description and prediction of experimental tumor growth. PLoS Comput Biol. 2014; 10(8):e1003800. Epub 2014/08/29. https://doi.org/10.1371/journal.pcbi.1003800 PMID: 25167199
27. Rafiei S, Komarova SV. Molecular signaling pathways mediating osteoclastogenesis induced by prostate cancer cells. BMC Cancer. 2013; 13:605. Epub 2013/12/29. https://doi.org/10.1186/1471-2407-13-605 PMID: 24370273
28. Lemaire V, Cox DR. Dynamics of Bone Cell Interactions and Differential Responses to PTH and Antibody-Based Therapies. Bull Math Biol. 2019; 81(9):3575–622. Epub 2018/11/22. https://doi.org/10.1007/s11538-018-0533-0 PMID: 30460589.

29. Akchurin T, Aissiou T, Kemeny N, Prosk E, Nigam N, Komarova SV. Complex dynamics of osteoclast formation and death in long-term cultures. PLoS One. 2008; 3(5):e2104. Epub 2008/05/08. https://doi.org/10.1371/journal.pone.0002104 PMID: 18461134

30. Buenzli PR, Jeon J, Pivonka P, Smith DW, Cummings PT. Investigation of bone resorption within a cortical basic multicellular unit using a lattice-based computational model. Bone. 2012; 50(1):378–89. Epub 2011/11/22. https://doi.org/10.1016/j.bone.2011.10.021 PMID: 22100414

31. Martinez-Reina J, Pivonka P. Effects of long-term treatment of denosumab on bone mineral density: insights from an in-silico model of bone mineralization. Bone. 2019; 125:87–95. Epub 2019/05/06. https://doi.org/10.1016/j.bone.2019.04.022 PMID: 31055117.

32. Komarova SV. Mathematical model of paracrine interactions between osteoclasts and osteoblasts predicts anabolic action of parathyroid hormone on bone. Endocrinology. 2005; 146(8):3589–95. Epub 2005/04/30. https://doi.org/10.1210/en.2004-1642 PMID: 15860557.

33. Pivonka P, Zimak J, Smith DW, Gardiner BS, Dunstan CR, Sims NA, et al. Model structure and control of bone remodeling: a theoretical study. Bone. 2008; 43(2):249–63. Epub 2008/06/03. https://doi.org/10.1016/j.bone.2008.03.025 PMID: 18514606.

34. Lemaire V, Tobin FL, Greller LD, Cho CR, Suva LJ. Modeling the interactions between osteoblast and osteoclast activities in bone remodeling. J Theor Biol. 2004; 229(3):293–309. Epub 2004/07/06. https://doi.org/10.1016/j.jtbi.2004.03.023 PMID: 15234198.

35. Ayati BP, Edwards CM, Webb GF, Wikswo JP. A mathematical model of bone remodeling dynamics for normal bone cell populations and myeloma bone disease. Biol Direct. 2010; 5:28. Epub 2010/04/22. https://doi.org/10.1186/1745-6150-5-28 PMID: 20406449

36. Buenzli PR, Pivonka P, Gardiner BS, Smith DW. Modelling the anabolic response of bone using a cell population model. J Theor Biol. 2012; 307:42–52. Epub 2012/05/15. https://doi.org/10.1016/j.jtbi.2012.04.019 PMID: 22579551.

37. Graham JM, Ayati BP, Holstein SA, Martin JA. The role of osteocytes in targeted bone remodeling: a mathematical model. PLoS One. 2013; 8(5):e63884. Epub 2013/05/30. https://doi.org/10.1371/journal.pone.0063884 PMID: 23717504

38. Bailon-Plaza A, van der Meulen MC. A mathematical framework to study the effects of growth factor influences on fracture healing. J Theor Biol. 2001; 212(2):191–209. Epub 2001/09/05. https://doi.org/10.1006/jtbi.2001.2372 PMID: 11531385.

39. Ryser MD, Nigam N, Komarova SV. Mathematical modeling of spatio-temporal dynamics of a single bone multicellular unit. J Bone Miner Res. 2009; 24(5):860–70. Epub 2008/12/10. https://doi.org/10.1359/jbmr.081229 PMID: 19063683.

40. Lo CH, Baratchart E, Basanta D, Lynch CC. Computational modeling reveals a key role for polarized myeloid cells in controlling osteoclast activity during bone injury repair. Sci Rep. 2021; 11(1):6055. Epub 2021/03/17. https://doi.org/10.1038/s41598-021-84888-1 PMID: 33723343

41. Trejo I, Kojouharov H, Chen-Charpentier B. Modeling the Macrophage-Mediated Inflammation Involved in the Bone Fracture Healing Process. Mathematical and Computational Applications. 2019; 24(1). https://doi.org/10.3390/mca24010012

42. Kojouharov HV, Trejo I, Chen-Charpentier BM. Modeling the effects of inflammation in bone fracture healing. AIP Conference Proceedings. 2017; 1895(1):020005. https://doi.org/10.1063/1.5007359

43. Aspenberg P, Sandberg O. Distal radial fractures heal by direct woven bone formation. Acta Orthop. 2013; 84(3):297–300. Epub 2013/04/11. https://doi.org/10.3109/17453674.2013.792769 PMID: 23570338

44. Chen WT, Han da C, Zhang PX, Han N, Kou YH, Yin XF, et al. A special healing pattern in stable metaphyseal fractures. Acta Orthop. 2015; 86(2):238–42. Epub 2015/01/15. https://doi.org/10.3109/17453674.2014.1003127 PMID: 25582035

45. Uhthoff HK, Rahn BA. Healing patterns of metaphyseal fractures. Clin Orthop Relat Res. 1981; (160):295–303. Epub 1981/10/01. PMID: 7285432.

46. Hiltunen A, Vuorio E, Aro HT. A standardized experimental fracture in the mouse tibia. J Orthop Res. 1993; 11(2):305–12. Epub 1993/03/01. https://doi.org/10.1002/jor.1100110219 PMID: 8483044.

47. Premnath P, Jorgenson B, Hess R, Tailor P, Louie D, Taiani J, et al. p21(-/-) mice exhibit enhanced bone regeneration after injury. BMC Musculoskelet Disord. 2017; 18(1):435. Epub 2017/11/11. https://doi.org/10.1186/s12891-017-1790-z PMID: 29121899

48. Taiani JT, Krawetz RJ, Yamashita A, Pauchard Y, Buie HR, Ponjevic D, et al. Embryonic stem cells incorporate into newly formed bone and do not form tumors in an immunocompetent mouse fracture model. Cell Transplant. 2013; 22(8):1453–62. Epub 2012/11/07. https://doi.org/10.3727/096368912X658755 PMID: 23127821.

49. Guihard P, Boutet MA, Brounais-Le Royer B, Gamblin AL, Amiaud J, Renaud A, et al. Oncostatin m, an inflammatory cytokine produced by macrophages, supports intramembranous bone healing in a

mouse model of tibia injury. Am J Pathol. 2015; 185(3):765–75. Epub 2015/01/07. https://doi.org/10.1016/j.ajpath.2014.11.008 PMID: 25559270.

50. Vi L, Baht GS, Whetstone H, Ng A, Wei Q, Poon R, et al. Macrophages promote osteoblastic differentiation in-vivo: implications in fracture repair and bone homeostasis. J Bone Miner Res. 2015; 30 (6):1090–102. Epub 2014/12/10. https://doi.org/10.1002/jbmr.2422 PMID: 25487241.

51. Kon T, Cho TJ, Aizawa T, Yamazaki M, Nooh N, Graves D, et al. Expression of osteoprotegerin, receptor activator of NF-kappaB ligand (osteoprotegerin ligand) and related proinflammatory cytokines during fracture healing. J Bone Miner Res. 2001; 16(6):1004–14. Epub 2001/06/08. https://doi.org/10.1359/jbmr.2001.16.6.1004 PMID: 11393777.

52. Misharin AV, Morales-Nebreda L, Mutlu GM, Budinger GR, Perlman H. Flow cytometric analysis of macrophages and dendritic cell subsets in the mouse lung. Am J Respir Cell Mol Biol. 2013; 49 (4):503–10. Epub 2013/05/16. https://doi.org/10.1165/rcmb.2013-0086MA PMID: 23672262

53. Liyanage SE, Gardner PJ, Ribeiro J, Cristante E, Sampson RD, Luhmann UF, et al. Flow cytometric analysis of inflammatory and resident myeloid populations in mouse ocular inflammatory models. Exp Eye Res. 2016; 151:160–70. Epub 2016/08/22. https://doi.org/10.1016/j.exer.2016.08.007 PMID: 27544307

54. Sunderkotter C, Nikolic T, Dillon MJ, Van Rooijen N, Stehling M, Drevets DA, et al. Subpopulations of mouse blood monocytes differ in maturation stage and inflammatory response. J Immunol. 2004; 172 (7):4410–7. Epub 2004/03/23. https://doi.org/10.4049/jimmunol.172.7.4410 PMID: 15034056.

55. Zhang X, Goncalves R, Mosser DM. The isolation and characterization of murine macrophages. Curr Protoc Immunol. 2008; Chapter 14:Unit 14 1. Epub 2008/11/20. https://doi.org/10.1002/0471142735.im1401s83 PMID: 19016445

56. Xue J, Schmidt SV, Sander J, Draffehn A, Krebs W, Quester I, et al. Transcriptome-based network analysis reveals a spectrum model of human macrophage activation. Immunity. 2014; 40(2):274–88. Epub 2014/02/18. https://doi.org/10.1016/j.immuni.2014.01.006 PMID: 24530056

57. Guilliams M, Mildner A, Yona S. Developmental and Functional Heterogeneity of Monocytes. Immunity. 2018; 49(4):595–613. Epub 2018/10/18. https://doi.org/10.1016/j.immuni.2018.10.005 PMID: 30332628.

58. Allen JE, Ruckerl D. The Silent Undertakers: Macrophages Programmed for Efferocytosis. Immunity. 2017; 47(5):810–2. Epub 2017/11/23. https://doi.org/10.1016/j.immuni.2017.10.010 PMID: 29166582.

59. Arango Duque G, Descoteaux A. Macrophage cytokines: involvement in immunity and infectious diseases. Front Immunol. 2014; 5:491. Epub 2014/10/24. https://doi.org/10.3389/fimmu.2014.00491 PMID: 25339958

60. BioRad Macrophage Polarization Mini Review. 2016.

61. Biswas SK, Gangi L, Paul S, Schioppa T, Saccani A, Sironi M, et al. A distinct and unique transcriptional program expressed by tumor-associated macrophages (defective NF-κB and enhanced IRF-3/STAT1 activation). Blood. 2006; 107(5):2112–22. https://doi.org/10.1182/blood-2005-01-0428 PMID: 16269622

62. Bronte V, Brandau S, Chen S-H, Colombo MP, Frey AB, Greten TF, et al. Recommendations for myeloid-derived suppressor cell nomenclature and characterization standards. Nature communications. 2016; 7(1):1–10. https://doi.org/10.1038/ncomms12150 PMID: 27381735

63. Broz ML, Binnewies M, Boldajipour B, Nelson AE, Pollack JL, Erle DJ, et al. Dissecting the tumor myeloid compartment reveals rare activating antigen-presenting cells critical for T cell immunity. Cancer cell. 2014; 26(5):638–52. https://doi.org/10.1016/j.ccell.2014.09.007 PMID: 25446897

64. Charles J.F. et al. Inflammatory arthritis increases mouse osteoclast precursors with myeloid suppressor function. The Journal of Clinical Investigation 122, 4592–4605. https://doi.org/10.1172/JCI60920 PMID: 23114597

65. Comito G, Giannoni E, Segura CP, Barcellos-de-Souza P, Raspollini MR, Baroni G, et al. Cancer-associated fibroblasts and M2-polarized macrophages synergize during prostate carcinoma progression. Oncogene. 2014; 33(19):2423–31. Epub 2013/06/04. https://doi.org/10.1038/onc.2013.191 PMID: 23728338.

66. Davies L.C., Jenkins S.J., Allen J.E. & Taylor P.R. Tissue-resident macrophages. Nature immunology 14, 986–995 (2013). https://doi.org/10.1038/ni.2705 PMID: 24048120

67. Davies LC, Taylor PR. Tissue-resident macrophages: then and now. Immunology. 2015; 144(4):541–8. https://doi.org/10.1111/imm.12451 PMID: 25684236

68. Davis MJ, Tsang TM, Qiu Y, Dayrit JK, Freij JB, Huffnagle GB, et al. Macrophage M1/M2 polarization dynamically adapts to changes in cytokine microenvironments in Cryptococcus neoformans infection. MBio. 2013; 4(3):e00264–13. https://doi.org/10.1128/mBio.00264-13 PMID: 23781069

69. de Bruin AM, Libregts SF, Valkhof M, Boon L, Touw IP, Nolte MA. IFNγ induces monopoiesis and inhibits neutrophil development during inflammation. Blood, The Journal of the American Society of Hematology. 2012; 119(6):1543–54. https://doi.org/10.1182/blood-2011-07-367706 PMID: 22117048

70. Francke A, Herold J, Weinert S, Strasser RH, Braun-Dullaeus RC. Generation of mature murine monocytes from heterogeneous bone marrow and description of their properties. Journal of Histochemistry & Cytochemistry. 2011; 59(9):813–25. https://doi.org/10.1369/0022155411416007 PMID: 21705645

71. Galea E, FEINSTEIN DL. Regulation of the expression of the inflammatory nitric oxide synthase (NOS2) by cyclic AMP. The FASEB Journal. 1999; 13(15):2125–37. https://doi.org/10.1096/fasebj.13.15.2125 PMID: 10593859

72. Göktuna SI, Canli O, Bollrath J, Fingerle AA, Horst D, Diamanti MA, et al. IKKα promotes intestinal tumorigenesis by limiting recruitment of M1-like polarized myeloid cells. Cell reports. 2014; 7(6):1914–25. https://doi.org/10.1016/j.celrep.2014.05.006 PMID: 24882009

73. Gomez Perdiguero E, Klapproth K, Schulz C, Busch K, Azzoni E, Crozet L, et al. Tissue-resident macrophages originate from yolk-sac-derived erythro-myeloid progenitors. Nature. 2015; 518(7540):547–51. https://doi.org/10.1038/nature13989 PMID: 25470051

74. Gordon S. Phagocytosis: the legacy of Metchnikoff. Cell. 2016; 166(5):1065–8. https://doi.org/10.1016/j.cell.2016.08.017 PMID: 27565334

75. Grivennikov SI, Greten FR, Karin M. Immunity, inflammation, and cancer. Cell. 2010; 140(6):883–99. Epub 2010/03/23. https://doi.org/10.1016/j.cell.2010.01.025 PMID: 20303878

76. Han CZ, Juncadella IJ, Kinchen JM, Buckley MW, Klibanov AL, Dryden K, et al. Macrophages redirect phagocytosis by non-professional phagocytes and influence inflammation. Nature. 2016; 539 (7630):570–4. https://doi.org/10.1038/nature20141 PMID: 27820945

77. He D, Kou X, Yang R, Liu D, Wang X, Luo Q, et al. M1-like Macrophage Polarization Promotes Orthodontic Tooth Movement. J Dent Res. 2015; 94(9):1286–94. Epub 2015/07/01. https://doi.org/10.1177/0022034515589714 PMID: 26124217.

78. Huang R, Wang X, Zhou Y, Xiao Y. RANKL-induced M1 macrophages are involved in bone formation. Bone Res. 2017; 5:17019. Epub 2017/12/22. https://doi.org/10.1038/boneres.2017.19 PMID: 29263936

79. Hussain SP, Trivers GE, Hofseth LJ, He P, Shaikh I, Mechanic LE, et al. Nitric oxide, a mediator of inflammation, suppresses tumorigenesis. Cancer Res. 2004; 64(19):6849–53. Epub 2004/10/07. https://doi.org/10.1158/0008-5472.CAN-04-2201 PMID: 15466171.

80. Italiani P, Boraschi D. From Monocytes to M1/M2 Macrophages: Phenotypical vs. Functional Differentiation. Front Immunol. 2014; 5:514. Epub 2014/11/05. https://doi.org/10.3389/fimmu.2014.00514 PMID: 25368618

81. Jeganathan S, Fiorino C, Naik U, Sun HS, Harrison RE. Modulation of osteoclastogenesis with macrophage M1- and M2-inducing stimuli. PLoS One. 2014; 9(8):e104498. Epub 2014/08/08. https://doi.org/10.1371/journal.pone.0104498 PMID: 25101660

82. Mattila JT, Thomas AC. Nitric oxide synthase: non-canonical expression patterns. Front Immunol. 2014; 5:478. Epub 2014/10/28. https://doi.org/10.3389/fimmu.2014.00478 PMID: 25346730

83. Kaur S, Raggatt LJ, Batoon L, Hume DA, Levesque JP, Pettit AR. Role of bone marrow macrophages in controlling homeostasis and repair in bone and bone marrow niches. Semin Cell Dev Biol. 2017; 61:12–21. Epub 2016/08/16. https://doi.org/10.1016/j.semcdb.2016.08.009 PMID: 27521519.

84. Koh TJ, DiPietro LA. Inflammation and wound healing: the role of the macrophage. Expert Rev Mol Med. 2011; 13:e23. Epub 2011/07/12. https://doi.org/10.1017/S1462399411001943 PMID: 21740602

85. Kratochvill F, Neale G, Haverkamp JM, Van de Velde LA, Smith AM, Kawauchi D, et al. TNF Counterbalances the Emergence of M2 Tumor Macrophages. Cell Rep. 2015; 12(11):1902–14. Epub 2015/09/15. https://doi.org/10.1016/j.celrep.2015.08.033 PMID: 26365184

86. Lampiasi N, Russo R, Zito F. The Alternative Faces of Macrophage Generate Osteoclasts. Biomed Res Int. 2016; 2016:9089610. Epub 2016/03/16. https://doi.org/10.1155/2016/9089610 PMID: 26977415

87. Liu YC, Zou XB, Chai YF, Yao YM. Macrophage polarization in inflammatory diseases. Int J Biol Sci. 2014; 10(5):520–9. Epub 2014/06/10. https://doi.org/10.7150/ijbs.8879 PMID: 24910531

88. Lo CH, Lynch CC. Multifaceted Roles for Macrophages in Prostate Cancer Skeletal Metastasis. Front Endocrinol (Lausanne). 2018; 9:247. Epub 2018/06/06. https://doi.org/10.3389/fendo.2018.00247 PMID: 29867776

89. Lu G, Zhang R, Geng S, Peng L, Jayaraman P, Chen C, et al. Myeloid cell-derived inducible nitric oxide synthase suppresses M1 macrophage polarization. Nature communications. 2015; 6(1):1–14. https://doi.org/10.1038/ncomms7676 PMID: 25813085

90. Mantovani A, Marchesi F, Malesci A, Laghi L, Allavena P. Tumour-associated macrophages as treatment targets in oncology. Nature reviews Clinical oncology. 2017; 14(7):399–416. https://doi.org/10.1038/nrclinonc.2016.217 PMID: 28117416

91. Martinez FO, Gordon S. The M1 and M2 paradigm of macrophage activation: time for reassessment. F1000Prime Rep. 2014; 6:13. Epub 2014/03/29. https://doi.org/10.12703/P6-13 PMID: 24669294

92. Mia S, Warnecke A, Zhang XM, Malmström V, Harris RA. An optimized protocol for human M2 macrophages using M-CSF and IL-4/IL-10/TGF-β yields a dominant immunosuppressive phenotype. Scandinavian journal of immunology. 2014; 79(5):305–14. https://doi.org/10.1111/sji.12162 PMID: 24521472

93. Michalski MN, Koh AJ, Weidner S, Roca H, McCauley LK. Modulation of Osteoblastic Cell Efferocytosis by Bone Marrow Macrophages. J Cell Biochem. 2016; 117(12):2697–706. Epub 2016/04/12. https://doi.org/10.1002/jcb.25567 PMID: 27061191

94. Michlewska S, Dransfield I, Megson IL, Rossi AG. Macrophage phagocytosis of apoptotic neutrophils is critically regulated by the opposing actions of pro-inflammatory and anti-inflammatory agents: key role for TNF-α. The FASEB Journal. 2009; 23(3):844–54. https://doi.org/10.1096/fj.08-121228 PMID: 18971259

95. Minutti CM, Knipper JA, Allen JE, Zaiss DM. Tissue-specific contribution of macrophages to wound healing. Semin Cell Dev Biol. 2017; 61:3–11. Epub 2016/08/16. https://doi.org/10.1016/j.semcdb.2016.08.006 PMID: 27521521.

96. Mosser DM, Edwards JP. Exploring the full spectrum of macrophage activation. Nat Rev Immunol. 2008; 8(12):958–69. Epub 2008/11/26. https://doi.org/10.1038/nri2448 PMID: 19029990

97. Naito M, Hasegawa G, Takahashi K. Development, differentiation, and maturation of Kupffer cells. Microsc Res Tech. 1997; 39(4):350–64. Epub 1998/01/04. https://doi.org/10.1002/(SICI)1097-0029(19971115)39:4<350::AID-JEMT5>3.0.CO;2-L PMID: 9407545.

98. Osta B, Benedetti G, Miossec P. Classical and Paradoxical Effects of TNF-alpha on Bone Homeostasis. Front Immunol. 2014; 5:48. Epub 2014/03/05. https://doi.org/10.3389/fimmu.2014.00048 PMID: 24592264

99. Rose S, Misharin A, Perlman H. A novel Ly6C/Ly6G-based strategy to analyze the mouse splenic myeloid compartment. Cytometry Part A. 2012; 81(4):343–50. https://doi.org/10.1002/cyto.a.22012 PMID: 22213571

100. Tan HY, Wang N, Li S, Hong M, Wang X, Feng Y. The Reactive Oxygen Species in Macrophage Polarization: Reflecting Its Dual Role in Progression and Treatment of Human Diseases. Oxid Med Cell Longev. 2016; 2016:2795090. Epub 2016/05/05. https://doi.org/10.1155/2016/2795090 PMID: 27143992

101. Van Epps HL. Macrophage activation unveiled. The Journal of Experimental Medicine. 2005; 202(7):884. https://doi.org/10.1084/jem.2027fta PMID: 16276563

102. Wang N, Liang H, Zen K. Molecular mechanisms that influence the macrophage M1–M2 polarization balance. Frontiers in immunology. 2014; 5:614. https://doi.org/10.3389/fimmu.2014.00614 PMID: 25506346

103. Yamaguchi T, Movila A, Kataoka S, Wisitrasameewong W, Ruiz Torruella M, Murakoshi M, et al. Proinflammatory M1 Macrophages Inhibit RANKL-Induced Osteoclastogenesis. Infect Immun. 2016; 84(10):2802–12. Epub 2016/07/28. https://doi.org/10.1128/IAI.00461-16 PMID: 27456834

104. Yin Y, Huang X, Lynn KD, Thorpe PE. Phosphatidylserine-targeting antibody induces M1 macrophage polarization and promotes myeloid-derived suppressor cell differentiation. Cancer immunology research. 2013; 1(4):256–68. https://doi.org/10.1158/2326-6066.CIR-13-0073 PMID: 24777853

105. Zhou D, Huang C, Lin Z, Zhan S, Kong L, Fang C, et al. Macrophage polarization and function with emphasis on the evolving roles of coordinated regulation of cellular signaling pathways. Cell Signal. 2014; 26(2):192–7. Epub 2013/11/14. https://doi.org/10.1016/j.cellsig.2013.11.004 PMID: 24219909.

106. Gerstenfeld LC, Cullinane DM, Barnes GL, Graves DT, Einhorn TA. Fracture healing as a post-natal developmental process: molecular, spatial, and temporal aspects of its regulation. J Cell Biochem. 2003; 88(5):873–84. Epub 2003/03/05. https://doi.org/10.1002/jcb.10435 PMID: 12616527.

107. Clermont G, Bartels J, Kumar R, Constantine G, Vodovotz Y, Chow C. In silico design of clinical trials: a method coming of age. Crit Care Med. 2004; 32(10):2061–70. Epub 2004/10/16. https://doi.org/10.1097/01.ccm.0000142394.28791.c3 PMID: 15483415.

108. Chow CC, Clermont G, Kumar R, Lagoa C, Tawadrous Z, Gallo D, et al. The acute inflammatory response in diverse shock states. Shock. 2005; 24(1):74–84. Epub 2005/07/01. https://doi.org/10.1097/01.shk.0000168526.97716.f3 PMID: 15988324.

109. Bendixen AC, Shevde NK, Dienger KM, Willson TM, Funk CD, Pike JW. IL-4 inhibits osteoclast formation through a direct action on osteoclast precursors via peroxisome proliferator-activated receptor γ1. Proceedings of the National Academy of Sciences. 2001; 98(5):2443–8.

110. Glass GE, Chan JK, Freidin A, Feldmann M, Horwood NJ, Nanchahal J. TNF-alpha promotes fracture repair by augmenting the recruitment and differentiation of muscle-derived stromal cells. Proc Natl Acad Sci U S A. 2011; 108(4):1585–90. Epub 2011/01/07. https://doi.org/10.1073/pnas.1018501108 PMID: 21209334

111. Hurst SM, Wilkinson TS, McLoughlin RM, Jones S, Horiuchi S, Yamamoto N, et al. Il-6 and its soluble receptor orchestrate a temporal switch in the pattern of leukocyte recruitment seen during acute inflammation. Immunity. 2001; 14(6):705–14. https://doi.org/10.1016/s1074-7613(01)00151-0 PMID: 11420041

112. Li X, Qin L, Bergenstock M, Bevelock LM, Novack DV, Partridge NC. Parathyroid hormone stimulates osteoblastic expression of MCP-1 to recruit and increase the fusion of pre/osteoclasts. Journal of biological chemistry. 2007; 282(45):33098–106.

113. Song L, Tan J, Wang Z, Ding P, Tang Q, Xia M, et al. Interleukin17A facilitates osteoclast differentiation and bone resorption via activation of autophagy in mouse bone marrow macrophages. Mol Med Rep. 2019; 19(6):4743–52. Epub 2019/05/07. https://doi.org/10.3892/mmr.2019.10155 PMID: 31059030

114. Yamada A, Takami M, Kawawa T, Yasuhara R, Zhao B, Mochizuki A, et al. Interleukin-4 inhibition of osteoclast differentiation is stronger than that of interleukin-13 and they are equivalent for induction of osteoprotegerin production from osteoblasts. Immunology. 2007; 120(4):573–9. https://doi.org/10.1111/j.1365-2567.2006.02538.x PMID: 17343616

115. Zhang Y-H, Heulsmann A, Tondravi MM, Mukherjee A, Abu-Amer Y. Tumor necrosis factor-α (TNF) stimulates RANKL-induced osteoclastogenesis via coupling of TNF type 1 receptor and RANK signaling pathways. Journal of Biological Chemistry. 2001; 276(1):563–8. https://doi.org/10.1074/jbc.M008198200 PMID: 11032840

116. Zhao Z, Hou X, Yin X, Li Y, Duan R, Boyce BF, et al. TNF induction of NF-κB RelB enhances RANKL-induced osteoclastogenesis by promoting inflammatory macrophage differentiation but also limits it through suppression of NFATc1 expression. PloS one. 2015; 10(8):e0135728. https://doi.org/10.1371/journal.pone.0135728 PMID: 26287732

117. Guihard P, Danger Y, Brounais B, David E, Brion R, Delecrin J, et al. Induction of osteogenesis in mesenchymal stem cells by activated monocytes/macrophages depends on oncostatin M signaling. Stem cells. 2012; 30(4):762–72. https://doi.org/10.1002/stem.1040 PMID: 22267310

118. Walker EC, McGregor NE, Poulton IJ, Solano M, Pompolo S, Fernandes TJ, et al. Oncostatin M promotes bone formation independently of resorption when signaling through leukemia inhibitory factor receptor in mice. The Journal of clinical investigation. 2010; 120(2):582–92. https://doi.org/10.1172/JCI40568 PMID: 20051625

119. Jay PR, Centrella M, Lorenzo J, Bruce A, Horowitz MC. Oncostatin-M: a new bone active cytokine that activates osteoblasts and inhibits bone resorption. Endocrinology. 1996; 137(4):1151–8. https://doi.org/10.1210/endo.137.4.8625883 PMID: 8625883

120. invitrogen Histostain-TRAcP Kit. 2007.

121. Fadok VA, Bratton DL, Konowal A, Freed PW, Westcott JY, Henson PM. Macrophages that have ingested apoptotic cells in vitro inhibit proinflammatory cytokine production through autocrine/paracrine mechanisms involving TGF-beta, PGE2, and PAF. J Clin Invest. 1998; 101(4):890–8. Epub 1998/03/21. https://doi.org/10.1172/JCI1112 PMID: 9466984

122. Smith TD, Tse MJ, Read EL, Liu WF. Regulation of macrophage polarization and plasticity by complex activation signals. Integr Biol (Camb). 2016; 8(9):946–55. Epub 2016/08/06. https://doi.org/10.1039/c6ib00105j PMID: 27492191

123. Eriksen EF. Cellular mechanisms of bone remodeling. Rev Endocr Metab Disord. 2010; 11(4):219–27. Epub 2010/12/29. https://doi.org/10.1007/s11154-010-9153-1 PMID: 21188536

124. Ryser MD, Murgas KA. Bone remodeling as a spatial evolutionary game. J Theor Biol. 2017; 418:16–26. Epub 2017/01/22. https://doi.org/10.1016/j.jtbi.2017.01.021 PMID: 28108306

125. Champagne CM, Takebe J, Offenbacher S, Cooper LF. Macrophage cell lines produce osteoinductive signals that include bone morphogenetic protein-2. Bone. 2002; 30(1):26–31. Epub 2002/01/17. https://doi.org/10.1016/s8756-3282(01)00638-x PMID: 11792561.

126. Jacome-Galarza CE, Lee SK, Lorenzo JA, Aguila HL. Identification, characterization, and isolation of a common progenitor for osteoclasts, macrophages, and dendritic cells from murine bone marrow and periphery. J Bone Miner Res. 2013; 28(5):1203–13. Epub 2012/11/21. https://doi.org/10.1002/jbmr.1822 PMID: 23165930

127. Cao Y, Jansen IDC, Sprangers S, Stap J, Leenen PJM, Everts V, et al. IL-1β differently stimulates proliferation and multinucleation of distinct mouse bone marrow osteoclast precursor subsets. Journal of Leukocyte Biology. 2016; 100(3%@ 0741–5400):513–23. https://jlb.onlinelibrary.wiley.com/doi/abs/10.1189/jlb.1A1215-543R. PMID: 26957213

128. Pereira M, Petretto E, Gordon S, Bassett JHD, Williams GR, Behmoaras J. Common signalling pathways in macrophage and osteoclast multinucleation. J Cell Sci. 2018; 131(11). Epub 2018/06/07. https://doi.org/10.1242/jcs.216267 PMID: 29871956.

129. Lam J, Takeshita S, Barker JE, Kanagawa O, Ross FP, Teitelbaum SL. TNF-alpha induces osteoclastogenesis by direct stimulation of macrophages exposed to permissive levels of RANK ligand. J Clin Invest. 2000; 106(12):1481–8. Epub 2000/12/20. https://doi.org/10.1172/JCI11176 PMID: 11120755

130. Kostenuik PJ. Osteoprotegerin and RANKL regulate bone resorption, density, geometry and strength. Curr Opin Pharmacol. 2005; 5(6):618–25. Epub 2005/09/29. https://doi.org/10.1016/j.coph.2005.06.005 PMID: 16188502.

131. Houde N, Chamoux E, Bisson M, Roux S. Transforming growth factor-beta1 (TGF-beta1) induces human osteoclast apoptosis by up-regulating Bim. J Biol Chem. 2009; 284(35):23397–404. Epub 2009/07/04. https://doi.org/10.1074/jbc.M109.019372 PMID: 19574221

132. Jimi E, Nakamura I, Duong LT, Ikebe T, Takahashi N, Rodan GA, et al. Interleukin 1 induces multinucleation and bone-resorbing activity of osteoclasts in the absence of osteoblasts/stromal cells. Exp Cell Res. 1999; 247(1):84–93. Epub 1999/02/27. https://doi.org/10.1006/excr.1998.4320 PMID: 10047450.

133. Steffen U, Schett G, Bozec A. How autoantibodies regulate osteoclast induced bone loss in rheumatoid arthritis. Frontiers in Immunology. 2019; 10:1483. https://doi.org/10.3389/fimmu.2019.01483 PMID: 31333647

134. Manolagas SC. Birth and death of bone cells: basic regulatory mechanisms and implications for the pathogenesis and treatment of osteoporosis. Endocrine reviews. 2000; 21(2):115–37. https://doi.org/10.1210/edrv.21.2.0395 PMID: 10782361

135. Wang L, Liu S, Zhao Y, Liu D, Liu Y, Chen C, et al. Osteoblast-induced osteoclast apoptosis by fas ligand/FAS pathway is required for maintenance of bone mass. Cell Death Differ. 2015; 22(10):1654–64. Epub 2015/03/07. https://doi.org/10.1038/cdd.2015.14 PMID: 25744024

136. Teti A. Mechanisms of osteoclast-dependent bone formation. BoneKEy reports. 2013; 2. https://doi.org/10.1038/bonekey.2013.183 PMID: 24422142

137. Zhang Z, Jimi E, Bothwell AL. Receptor activator of NF-κB ligand stimulates recruitment of SHP-1 to the complex containing TNFR-associated factor 6 that regulates osteoclastogenesis. The Journal of Immunology. 2003; 171(7):3620–6. https://doi.org/10.4049/jimmunol.171.7.3620 PMID: 14500659

138. Takeshita S, Kaji K, Kudo A. Identification and characterization of the new osteoclast progenitor with macrophage phenotypes being able to differentiate into mature osteoclasts. Journal of Bone and Mineral Research. 2000; 15(8):1477–88. https://doi.org/10.1359/jbmr.2000.15.8.1477 PMID: 10934646

139. Bozec A, Soulat D. Latest perspectives on macrophages in bone homeostasis. Pflügers Archiv-European Journal of Physiology. 2017; 469(3):517–25. https://doi.org/10.1007/s00424-017-1952-8 PMID: 28247013

140. Pollard JW. Trophic macrophages in development and disease. Nature reviews immunology. 2009; 9(4):259–70. https://doi.org/10.1038/nri2528 PMID: 19282852

141. Campbell T, Wong W, Mackie E. Establishment of a model of cortical bone repair in mice. Calcified tissue international. 2003; 73(1):49–55. https://doi.org/10.1007/s00223-002-2120-4 PMID: 14506954

142. Alexander KA, Raggatt LJ, Millard S, Batoon L, Chiu-Ku Wu A, Chang MK, et al. Resting and injury-induced inflamed periosteum contain multiple macrophage subsets that are located at sites of bone growth and regeneration. Immunology and cell biology. 2017; 95(1):7–16. https://doi.org/10.1038/icb.2016.74 PMID: 27553584

143. Pettit AR, Chang MK, Hume DA, Raggatt L-J. Osteal macrophages: a new twist on coupling during bone dynamics. Bone. 2008; 43(6):976–82. https://doi.org/10.1016/j.bone.2008.08.128 PMID: 18835590

144. Udagawa N, Takahashi N, Jimi E, Matsuzaki K, Tsurukai T, Itoh K, et al. Osteoblasts/stromal cells stimulate osteoclast activation through expression of osteoclast differentiation factor/RANKL but not macrophage colony-stimulating factor. Bone. 1999; 25(5):517–23. https://doi.org/10.1016/s8756-3282(99)00210-0 PMID: 10574571

145. Estus TL, Choudhary S, Pilbeam CC. Prostaglandin-mediated inhibition of PTH-stimulated β-catenin signaling in osteoblasts by bone marrow macrophages. Bone. 2016; 85:123–30. https://doi.org/10.1016/j.bone.2016.01.023 PMID: 26851123

146. Sinder BP, Zweifler L, Koh AJ, Michalski MN, Hofbauer LC, Aguirre JI, et al. Bone mass is compromised by the chemotherapeutic trabectedin in association with effects on osteoblasts and macrophage efferocytosis. Journal of Bone and Mineral Research. 2017; 32(10):2116–27. https://doi.org/10.1002/jbmr.3196 PMID: 28600866

147. Crane MJ, Daley JM, van Houtte O, Brancato SK, Henry WL Jr, Albina JE. The monocyte to macrophage transition in the murine sterile wound. PloS one. 2014; 9(1):e86660. https://doi.org/10.1371/journal.pone.0086660 PMID: 24466192

148. Das A, Ganesh K, Khanna S, Sen CK, Roy S. Engulfment of apoptotic cells by macrophages: a role of microRNA-21 in the resolution of wound inflammation. The Journal of Immunology. 2014; 192 (3):1120–9. https://doi.org/10.4049/jimmunol.1300613 PMID: 24391209

149. Arienti S, Barth ND, Dorward DA, Rossi AG, Dransfield I. Regulation of apoptotic cell clearance during resolution of inflammation. Frontiers in pharmacology. 2019: 891. https://doi.org/10.3389/fphar.2019.00891 PMID: 31456686

150. Cho SW. Role of osteal macrophages in bone metabolism. Journal of pathology and translational medicine. 2015; 49(2):102. https://doi.org/10.4132/jptm.2015.02.02 PMID: 25812731

151. Schlitzer A, Schultze JL. Tissue-resident macrophages—how to humanize our knowledge. Immunology and cell biology. 2017; 95(2):173–7. https://doi.org/10.1038/icb.2016.82 PMID: 27752049

152. van de Laar L, Saelens W, De Prijck S, Martens L, Scott CL, Van Isterdael G, et al. Yolk sac macrophages, fetal liver, and adult monocytes can colonize an empty niche and develop into functional tissue-resident macrophages. Immunity. 2016; 44(4):755–68. https://doi.org/10.1016/j.immuni.2016.02.017 PMID: 26992565

153. Campana L, Lewis PJS, Pellicoro A, Aucott RL, Man J, O'Duibhir E, et al. The STAT3–IL-10–IL-6 pathway is a novel regulator of macrophage efferocytosis and phenotypic conversion in sterile liver injury. The Journal of Immunology. 2018; 200(3):1169–87. https://doi.org/10.4049/jimmunol.1701247 PMID: 29263216

154. Chang C-F, Goods BA, Askenase MH, Hammond MD, Renfroe SC, Steinschneider AF, et al. Erythrocyte efferocytosis modulates macrophages towards recovery after intracerebral hemorrhage. The Journal of clinical investigation. 2018; 128(2):607–24. https://doi.org/10.1172/JCI95612 PMID: 29251628

155. Rajfer RA, Flores M, Abraham A, Garcia E, Hinojosa N, Desai M, et al. Prevention of osteoporosis in the ovariectomized rat by oral administration of a nutraceutical combination that stimulates nitric oxide production. Journal of osteoporosis. 2019 https://doi.org/10.1155/2019/1592328 PMID: 31275540

156. Levaot N, Ottolenghi A, Mann M, Guterman-Ram G, Kam Z, Geiger B. Osteoclast fusion is initiated by a small subset of RANKL-stimulated monocyte progenitors, which can fuse to RANKL-unstimulated progenitors. Bone. 2015; 79:21–8. https://doi.org/10.1016/j.bone.2015.05.021 PMID: 26008608

157. Grundnes O, Reikerås O. The importance of the hematoma for fracture healing in rats. Acta orthopaedica Scandinavica. 1993; 64(3):340–2. https://doi.org/10.3109/17453679308993640 PMID: 8322595

158. Patel AA, Zhang Y, Fullerton JN, Boelen L, Rongvaux A, Maini AA, et al. The fate and lifespan of human monocyte subsets in steady state and systemic inflammation. Journal of Experimental Medicine. 2017; 214(7):1913–23. https://doi.org/10.1084/jem.20170355 PMID: 28606987

159. Yona S, Kim K-W, Wolf Y, Mildner A, Varol D, Breker M, et al. Fate mapping reveals origins and dynamics of monocytes and tissue macrophages under homeostasis. Immunity. 2013; 38(1):79–91. https://doi.org/10.1016/j.immuni.2012.12.001 PMID: 23273845

160. Wei W, Zeve D, Wang X, Du Y, Tang W, Dechow PC, et al. Osteoclast progenitors reside in the peroxisome proliferator-activated receptor gamma-expressing bone marrow cell population. Mol Cell Biol. 2011; 31(23):4692–705. Epub 2011/09/29. https://doi.org/10.1128/MCB.05979-11 PMID: 21947280